J. Fluid Mech. (2011), *vol.* 688, *pp.* 219–257.
doi:10.1017/jfm.2011.374

Probability density function approach for modelling multi-phase flow with ganglia in porous media

Manav Tyagi† and Patrick Jenny

Institute of Fluid Dynamics, Sonneggstrasse 3, ETH Zurich, Zuerich, CH8092, Switzerland

(Received 20 May 2010; revised 14 June 2011; accepted 5 September 2011;
first published online 17 October 2011)

A probabilistic approach to model macroscopic behaviour of non-wetting-phase ganglia or blobs in multi-phase flow through porous media is proposed. The key idea is to consider a set of stochastic Markov processes that can mimic the microscopic multi-phase dynamics. These processes are characterized by equilibrium probability density functions (PDFs) and correlation times, which can be obtained from micro-scale simulation studies or experiments. A Lagrangian viewpoint is adopted, where stochastic particles represent infinitesimal fluid elements and evolve in the physical and probability space. Ganglion mobilization and trapping are modelled by a two-state jump process with transition probabilities given as functions of ganglion size. Coalescence and breakup of ganglia influence the ganglion size distribution, which is modelled by a Langevin type equation. The joint probability density function (JPDF) of the chosen stochastic variables is governed by a high-dimensional Chapman–Kolmogorov equation. This equation can be used to derive moment (e.g. saturation, mean mobility etc.) transport equations, which in general do not form a closed system. However, in some special cases, which arise in the limit of one time scale being smaller or larger than the others, a closed set of moment transport equations can be obtained. For slowly varying and quasi-uniform flows, the saturation transport equation appears in closed form with the mean mobility fully determined, if the equilibrium PDFs are known. Furthermore, it is shown how statistical parameters such as mobilization and trapping rates and equilibrium PDFs can be obtained from the birth–death type approach, in which ganglia breakup and coalescence are explicitly considered. A two-equation transport model (one equation for the total saturation and one for the trapped saturation) is obtained in the limit of very fast coalescence and breakup processes. This model is employed to mimic hysteresis in relative permeability–saturation curves; a well known phenomenon observed in the successive processes of imbibition and drainage. For the general case, the JPDF-equation is solved using the stochastic particle method, which was proposed in our previous paper (Tyagi *et al. J. Comput. Phys.* **227**, 2008, 6696–6714). Several one- and two-dimensional numerical simulation results are presented to show the influence of correlation times on the averaged macroscopic flow behaviour.

Key words: breakup/coalescence, multiphase flow, porous media

† Email address for correspondence: tyagi@ifd.mavt.ethz.ch

1. Introduction

Geological flows often consist of multiple phases, which interact in a very complex and nonlinear fashion among each other and with the rock. The highly heterogeneous and anisotropic nature of subsurface formations further complicates the flow physics. A few important examples of such flows include: water–oil–gas flow (three phases) in oil reservoirs and CO_2–brine flow (two phases) during CO_2 storage in saline aquifers. For an accurate flow prediction, the constitutive models must properly account for the relevant flow physics. While governing equations for flow at the pore scale are well-known, they are of little value to simulate realistic field-scale scenarios (ratio of $\sim 10^9$ from field to pore scales). Therefore, in order to make flow simulations computationally feasible for realistic domains, one requires upscaled models, e.g. balance equations for phase saturations, which are defined as averages over a representative elementary volume (REV). The average pore-scale flow is modelled via certain macroscopic parameters, which can, for example, be obtained from experiments or pore-scale simulations. Currently, for momentum balance most of the upscaled flow models employ Darcy's law, which was initially proposed for single-phase flow and later extended for multi-phase flow (Muskat 1949). However, this leads to a rather ad hoc description. For multi-phase flow in an isotropic porous medium with the rock permeability k Darcy's law reads (neglecting macroscopic capillary pressure effects) (Bear 1972)

$$\boldsymbol{F}_a = -\frac{k_{ra}k}{\mu_a}(\nabla p + \rho_a g \boldsymbol{e}_z), \tag{1.1}$$

where p is the pressure and $\boldsymbol{F}_a$, k_{ra}, μ_a and ρ_a are the volume flux, relative permeability, viscosity and density, respectively, of phase a. The gravitational acceleration g is assumed to be directed along the negative z-axis, where ez is a unit vector parallel to the z-axis. The relative permeabilities are usually expressed as functions of macroscopic phase volume fraction (saturation S_a).

The concept of relative permeability and the assumption that it depends only on saturation has remained one of the main longstanding criticisms of (1.1). In laboratory measurements and pore-network simulations, it has been observed that relative permeabilities also depend on, for example, flow direction (imbibition or drainage) and the flow history (Lenormand, Zarcone & Sarr 1983; Jerauld & Salter 1990). This phenomenon is known as relative permeability hysteresis, which results in non-unique k_r–S curves. At pore scale, this hysteresis has two main sources: first, the contact angles are different at the advancing and the receding fronts and second, the oil phase gets disconnected into blobs or ganglia (Lenhard, Parker & Kaluarcchchi 1989; de Gennes, Brochard-Wyart & Quere 2004). Non-wetting-phase ganglia are formed during imbibition by capillary snap-off (oil-neck rupture), which is a pore-scale phenomenon and was first studied by Roof (1970). In the present work we focus on the second source of hysteresis, which is often the main mechanism (true for consolidated porous media) (see e.g. Lenhard *et al.* 1989; Kats & Dujin 2001).

There exist many practical scenarios where ganglia formation and their subsequent motion have a significant influence on the flow dynamics. For instance, during enhanced oil recovery (EOR), after the primary and secondary oil production stages, 40–80 % of the oil remains entrapped as ganglia, whereas the ganglion size typically varies from one to fifteen elemental chamber volumes (Payatakes 1982). Various techniques to mobilize these oil ganglia (including the use of surfactants) have been introduced in the oil industry, and their further development remains an important field of research. Another important example where ganglia formation plays a crucial role

is CO_2 storage. Recently, capillary entrapment or residual trapping has been identified as one of the important mechanisms for CO_2 storage in brine aquifers (Kumar *et al.* 2005; Juanes *et al.* 2006; Ide, Jessen & Orr 2007). After the injection of supercritical CO_2 into a brine aquifer, the buoyant CO_2 plume migrates vertically upwards. At the leading edge of the plume, the CO_2 phase displaces the wetting brine phase (drainage) and in the trailing region of the plume, the brine phase displaces the CO_2 phase (imbibition) leading to disconnected CO_2 ganglia. If capillary forces on a ganglion dominate over the viscous and buoyant forces, it gets trapped. With a first-order estimate analysis Hesse, Orr & Tchelepi (2008) showed that a significant fraction of CO_2 can be stored by this mechanism, in particular if the aquifer is slightly inclined.

In the porous media community there exists a longstanding misconception that non-wetting-phase ganglia always get trapped and only the part of the phase with connected pathways can move (Richards 1931; Dullien 1992). Hence, it is assumed that the saturation below which the non-wetting phase is disconnected is equal to the residual saturation. However, this is true only if the capillary number is infinitesimal, i.e. in the capillary equilibrium, in which case percolation theory can be used to calculate the residual saturation. It is known that for flows with finite capillary numbers, only a fraction of ganglia gets trapped. Larson, Scriven & Davis (1977) analytically showed that for a given pore geometry and topology, the critical length of a ganglion below which it can get trapped is inversely proportional to the capillary number. Since ganglion size has a distribution, the residual saturation (fraction of immobile ganglia volume) is only a fraction of the actual non-wetting-phase saturation. In the past three decades, there has been a lot of experimental and computational work to support this fact, notably the work of Payatakes and his co-workers (Ng, Davis & Scriven 1978; Payatakes 1982; Wardlaw & McKellar 1985; Gioia, Alfani, Andreutti & Murena 2003). For example, Avraam *et al.* (1994) and Avraam & Payatakes (1995*a*) performed experiments over a wide range of parameters for steady-state two-phase flow and showed that the disconnected oil ganglia contribute substantially to the oil flow. They found that the nature of ganglia flow depends on the capillary number, viscosity ratio and water saturation, and that it has a strong influence on the relative permeability of oil. We argue that such a deep understanding of ganglion dynamics is important in order to build more accurate macroscopic multi-phase flow models.

In an excellent review by Payatakes (1982) on the motion of oil ganglia the following definition of a ganglion can be found: ‘A ganglion is a nodular blob of a non-wetting phase that occupies at least one and usually several adjoining chambers of the void space in a permeable media’. The average velocity of a solitary ganglion is determined by the resultant of capillary, viscous and buoyant forces acting upon it. For a given flow, the pore space topology and the ganglion shape and size determine the relative magnitude of these forces. Dias & Payatakes (1986*a*,*b*) studied the motion of a solitary oil ganglion with the help of pore-network simulations for a wide range of capillary numbers. More recently, Amili & Yortsos (2006) devised a new approach called ‘Darcian dynamics’ to study the motion of ganglia populations, where the interaction among ganglia is also taken into account. A ganglion moves in a discontinuous fashion experiencing a sequence of mobilization and trapping events. Further, a ganglion can break up into two (or more) daughter ganglia and collision of two (or more) ganglia may lead to coalescence, thus forming a bigger ganglion. Monte Carlo simulations of these events provide the statistical information, which can be used for macroscopic models (Ng & Payatakes 1980).

A macroscopic description of ganglia flow can be given by birth–death type population balance equations, which are formulated for the size distribution functions

of the subpopulations of mobile and trapped ganglia (Payatakes, Nag & Flumerfelt 1980). This approach assumes that pore-scale events such as ganglion mobilization, trapping, breakup and coalescence are discontinuous stochastic Markov processes. This is analogous to the statistical description of molecular dynamics by the Boltzmann equation (Cercignani 1988). The input information required by the population balance equations are the rates of various processes as functions of ganglion size. Valavanides, Constantinides & Payatakes (1998) solved population balance equations for steady-state fully and non-fully developed one-dimensional flows. Their results showed a strong influence of viscosity ratio and coalescence factor on the macroscopic flow (e.g. on the relative permeabilities), based on which they concluded that there exists a strong nonlinear relationship between the applied macroscopic pressure gradient and the superficial velocities of oil and water.

Although a birth–death type approach can be considered as the most basic statistical framework to describe a flowing ganglion population, its application to realistic field-scale flows is limited for the following reasons. First, due to the explicit modelling of ganglion coalescence and breakup, the computational effort varies quadratically with the grid size, thus making the method tremendously expensive for large grids (e.g. in two and three dimensions). Second, there is no way to determine macroscopic pressure gradient from population balance equations; this would be a serious limitation, if the method were used to simulate subsurface flows (see Valavanides *et al.* 1998, p. 289). Third, in a birth–death model, one needs to resolve length and time scales associated with breakup and coalescence processes; consequently, the time step size in a simulation is limited.

The present paper proposes an alternative probability density function (PDF)-based framework in which one can easily model the influence of microscopic ganglion dynamics on the macroscopic flow. The basic idea is to describe the flow by a set of stochastic Markov processes mimicking the pore-scale multi-phase flow dynamics. The framework allows us to approximate the discontinuous processes of coalescence and breakup by a continuous process, where the latter can be handled much more efficiently during computer simulations. The evolution of the joint probability density function (JPDF) of relevant stochastic variables is governed by a differential Chapman–Kolmogorov equation (DCKE), which consists of convection, diffusion and source terms in a high-dimensional (physical plus probability) space (Gardiner 2004). The coefficients in the DCKE are obtained from the Lagrangian evolution of the stochastic variables. Similar PDF-based methods have successfully been applied in many other fields of science and engineering; for example, in turbulent combustion modelling, where the PDF-method has the advantage compared with Reynolds averaged Navier–Stokes (RANS) models that nonlinear reaction, Reynolds stress convection and scalar transport appear in closed form (Pope 1985, 2003).

The present stochastic model considers ganglia jumping from mobile to trapped states and vice versa. The corresponding transitional probabilities are assumed to be functions of ganglion size, which itself evolves according to a continuous stochastic Markov process. Here, a Langevin equation, which is characterized by an equilibrium mean ganglion size, a relaxation time and an equilibrium variance, is employed to model the ganglion size distribution. The velocity of a mobile ganglion is assumed to be proportional to the gradient of a macroscopic pressure, which is obtained from the average mass balance. Each process, i.e. flow, mobilization–trapping and coalescence–breakup, has its own characteristic time scale. Special cases of the DCKE were derived by assuming certain time scales very small or very large. These asymptotic equations provide additional insight and some of them can be linked to

the previously proposed models (see Hassanizadeh, Celia & Dahle 2002; Barenblatt, Patzek & Silin 2003; Hilfer 2006*b*; Tyagi *et al.* 2008, for example).

Although in principle the JPDF-evolution equation can be solved numerically, for example by employing a finite volume method, the computational effort would be tremendous since the JPDF evolves in a high-dimensional space (3 + number of independent probability space dimensions). An alternative approach is to employ computational particles and evolve them in the joint physical and probability space with the Lagrangian model equations. These particles represent infinitesimal fluid elements and evolve such that their statistics represent the statistics of the physical fluid elements. Note that numerically the particle ensemble in a grid cell represents the JPDF at that location. Tyagi *et al.* (2008) developed the stochastic particle method (SPM) for simulating multi-phase flow in porous media, which is an extension of the particle method for single-phase flows (Ahlstrom *et al.* 1977; Prickett, Naymik & Longquist 1981; Kinzelbach 1992), and demonstrated its consistency and convergence. The following list outlines some important properties of the SPM that distinguish it from other particle methods for multi-phase flow such as the ones based on the method of characteristics (Dahle *et al.* 1990; Dahle, Ewing & Russell 1995; Hewett & Yamada 1997). (i) A particle belongs to a phase, i.e. in an n-phase flow, there exist n-kinds of particles. (ii) Saturation is defined over an ensemble of particles and is not a particle property. (iii) A particle moves in physical space with a velocity such that the phase volume flux is equal to the conditional expectation of the particle velocity times porosity times saturation. Particles can carry other variables, which evolve in their corresponding sample spaces as the particles move. For example, in Tyagi *et al.* (2008) we chose mobility as a particle property, and modelled its Lagrangian evolution by a Langevin equation. The presence of finite correlation time in the mobility model gives rise to non-equilibrium fluxes that relax towards the equilibrium values at a rate equal to the inverse of the correlation time.

The main goals of the present paper are: to outline the basic mathematical framework necessary to model multi-phase flow with ganglia in porous media and to demonstrate its utility with the help of some examples. These examples are chosen such that the modelling capabilities and the advantages of the framework over existing modelling approaches can be demonstrated. Throughout the paper, the emphasis is on describing a modelling approach which allows us to consider various pore-scale phenomena in a consistent and natural way. To achieve quantitative agreement with experiments or field-scale measurements, one needs to calibrate certain parameters or modify/add stochastic processes according to the relevant pore-scale dynamics. This issue is briefly addressed in § 8 and in appendix A and will be the focus of future work.

The paper is organized as follows. First, in § 2, based on the microscopic ganglion dynamics the Lagrangian evolution of relevant stochastic variables is developed. Next, in § 3, the notions of JPDF and MDF (mass density function) are introduced in the context of multi-phase flow in porous media and their evolution equations are derived. Further, in the same section, the MDF-transport equation is used to derive transport equations, which in general, however, are unclosed, for stochastic moments. This section also includes the derivation of the pressure equation and the identification of various time scales. Section 4 considers the special case of slow or quasi-uniform flow, where several simplified forms of the JPDF-equation are derived. Section 5 investigates the case of rapid coalescence and breakup, which leads to a closed system of stochastic moment equations. In § 6, the case of rapid mobilization and trapping, which leads to a continuous stochastic velocity, is discussed. The results are presented

in § 7 and a brief discussion of some modelling issues follows in § 8. Finally, in § 9, the conclusions are drawn. Additionally, in appendix A it is shown how micro-scale information can be used to derive modelling parameters in the PDF-approach and in appendix B a simplified model for the well-known relative permeability hysteresis is derived.

2. Lagrangian stochastic model

Consider a flow of many immiscible phases in a porous medium at a sufficiently low velocity such that it remains in the Stokes regime. Here, the evolution of individual infinitesimal fluid elements in the pore space is described by an ensemble of stochastic particles. The assumption here is that the deterministic system of evolving fluid elements is statistically equivalent to the system of stochastic particles. In a stochastic model, it is crucial to choose an appropriate probability space and to determine appropriate stochastic processes which can accurately represent the Lagrangian statistics of the actual microscopic flow. The properties of a stochastic particle may consist of a phase indicator $A(t)$, a position $\boldsymbol{X}(t)$, a velocity $\boldsymbol{U}(t)$, a mobility $\Lambda(t)$, a mass $M(t)$ and the size $V(t)$ of the connected volume. Below we propose models for these particle properties, where we consider the fine-scale physics of multi-phase flow in the pore space. For simplicity we do not consider miscibility and phase changes; thus the phase of a particle is preserved, i.e.

$$A(t) = A(0), \tag{2.1}$$

where $A(0)$ is the particle phase at $t = 0$. Note that, for mathematical subtlety, A is still written as a (constant) function of time; this will help us in formulating a single joint distribution function of all phases together.

2.1. *Particle position*

We model particle evolution in physical space with the stochastic differential equation (SDE) (Tyagi *et al.* 2008; Tyagi & Jenny 2011)

$$\mathrm{d}\boldsymbol{X}(t) = \underbrace{\boldsymbol{U}(t)\,\mathrm{d}t}_{drift} + \underbrace{\sqrt{2\Gamma|\boldsymbol{U}(t)|}\,\mathrm{d}\boldsymbol{W}(t)}_{diffusion}, \tag{2.2}$$

where $\boldsymbol{W}(t) \equiv \{W_1(t), W_2(t), W_3(t)\}^{\mathrm{T}}$ is a Wiener process with $\langle \mathrm{d}W_i \rangle = 0$ and $\langle \mathrm{d}W_i\,\mathrm{d}W_j \rangle = \delta_{ij}\,\mathrm{d}t$, and Γ is a dispersion coefficient depicting the pore space network topology. The drift term describes the expected displacement of the actual fluid element and the diffusion term mimics the stochastic displacement due to pore-scale inhomogeneities (variance of the stochastic displacement is proportional to the magnitude of expected displacement). It must be emphasized that the pore-scale dispersion model considered here is one of the simplest (for example, see Bear 1972) and it does not incorporate non-Markovian (and non-Fickian) effects and nonlinear velocity dependence (de Gennes 1983; Koch & Brady 1987). However, the focus of the present paper is not to propose an accurate pore-scale dispersion model, but to develop a stochastic framework for modelling ganglia flow in porous media. Since these flows are often dominated by convection, inaccuracies due to the dispersion model can safely be ignored.

2.2. *Particle velocity*

Except for some very special cases it is widely accepted and well established that for single-phase flow in porous media Darcy's law is a good approximation for the

average fluid velocity. Therefore, in the absence of other phases, we assume that $\boldsymbol{U}$ is governed by Darcy's law. To account for the influence of other phases on the particle motion, we multiply this velocity by the individual mobility Λ, i.e. for multi-phase flow we write

$$\boldsymbol{U} = -\Lambda \frac{k}{\phi \mu_A} (\boldsymbol{\nabla} p_A + \rho_A g \boldsymbol{e}_z), \tag{2.3}$$

where k is the rock permeability, ϕ is the porosity and μ_A, p_A and ρ_A are the viscosity, pressure and density of the particle, respectively. The phase pressure p_A is approximated as an average Eulerian quantity. Further, the viscosity and density of a phase are assumed to be constant.

2.3. *Particle mobility*

Depending on the flow conditions and structure of the porous medium, a phase can either be connected or be present in the form of disconnected ganglia. Such ganglia undergo discontinuous motions alternating between mobile and trapped states. To model the microscopic motion of a ganglion in our stochastic framework, we consider a stochastic particle (representing the ganglion) with either $\Lambda \neq 0$ (mobile) or $\Lambda = 0$ (trapped). While a general non-equilibrium model for the mobility of the mobile particle could be employed (e.g. as proposed in Tyagi *et al.* (2008)), here $\Lambda = k_{r_A}/S_A$ is used for the mobile ganglia (S_A and k_{r_A} are the saturation and relative permeability, respectively, of phase A). Consequently, the mobility can be written as

$$\Lambda = \frac{k_{r_A}}{S_A} N, \tag{2.4}$$

where

$$N = \begin{cases} 0, & \text{if the particle is trapped} \\ 1, & \text{if the particle is mobile} \end{cases} \tag{2.5}$$

is another particle property. Transition from one state to the other is modelled via the transition probabilities

$$\text{Prob}(N : 0 \to 1; \mathrm{d}t) = \alpha_M \, \mathrm{d}t \quad \text{and} \quad \text{Prob}(N : 1 \to 0; \mathrm{d}t) = \alpha_T \, \mathrm{d}t, \tag{2.6}$$

where α_T and α_M are trapping and mobilization rates, which are flow and ganglion-size dependent (Ng & Payatakes 1980). In appendix A, we show how these rates can be obtained from birth–death type population balance equations (Payatakes *et al.* 1980).

2.4. *Particle size*

In a flow, a ganglion undergoes a sequence of coalescence and breakup events, which dynamically influence the ganglion size distribution (Avraam & Payatakes 1995*a*). A statistical description of such a scenario can be given by birth–death type population balance equations (Payatakes *et al.* 1980). However, solving the resulting integro-differential equations directly can computationally be very expensive (Valavanides *et al.* 1998). Alternatively, a Monte Carlo method, where coalescence and breakup probabilities are employed, can be used. Though in principle this method could be implemented in our stochastic particle framework, it is still computationally very expensive. Moreover, a birth–death type model requires resolving the actual microscopic time scale of coalescence and breakup. Therefore, this mesoscopic simulation approach is limited to small samples sizes. To avoid these

difficulties and be able to simulate realistic large-scale subsurface flow, we propose an alternative approach where the ganglion size distribution is modelled by a continuous stochastic Markov process. The validity of this approximation will be examined in appendix A. Such an approach has been employed in many other fields of science and engineering, where a birth–death (Master) or Boltzmann equation is approximated by a Fokker–Planck equation. An example of this is the Fokker–Planck model for the motion of a rarefied gas as an approximation to the Boltzmann equation (Heinz 2004; Jenny, Torrilhon & Heinz 2010). If the Wiener process is used to model random fluctuations, the stochastic evolution of ganglion size, V, can be described by a generalized Langevin equation

$$\mathrm{d}V(t) = D^{v}\,\mathrm{d}t + \sqrt{2D^{v,v}}\,\mathrm{d}W(t), \tag{2.7}$$

where D^{v} is the conditional velocity and $D^{v,v}$ is the isotropic diffusion coefficient in the Fokker–Planck equation, which governs the PDF of V in v-space. Note that the Wiener process $W(t)$ employed here is independent of the one appearing in the particle displacement model (2.2).

One of the physical requirements for the ganglion size process is that it has to remain non-negative. This can be achieved via an appropriate mapping from another stochastic variable χ to V, where χ evolves according to the Ornstein–Uhlenbeck process (Gardiner 2004)

$$\mathrm{d}\chi(t) = -\frac{\chi(t)}{\tau_v}\,\mathrm{d}t + \sqrt{\frac{2\sigma^2}{\tau_v}}\,\mathrm{d}W(t). \tag{2.8}$$

Note that τ_v is the characteristic relaxation time and that the stationary solution of (2.8) has a Gaussian distribution (if τ_v and σ are independent of χ) with zero mean and variance σ^2. In the present paper, the mapping

$$V = V^{eq}\mathrm{e}^{\{\chi-\sigma^2/2\}}, \tag{2.9}$$

is employed, which (if χ is Gaussian) leads to a log-normal distribution of V with mean V^{eq} and variance $V^{eq^2}\{\exp(\sigma^2)-1\}$. The evolution of V is governed by

$$\mathrm{d}V(t) = -\frac{V(t)}{\tau_v}\left\{\log\left(\frac{V(t)}{V^{eq}}\right) - \frac{\sigma^2}{2}\right\}\mathrm{d}t + V(t)\sqrt{\frac{2\sigma^2}{\tau_v}}\,\mathrm{d}W(t), \tag{2.10}$$

which can be derived using the Itō transformation (Gardiner 2004). It has to be emphasized that the mapping (2.9), which leads to a log-normal equilibrium distribution of V, is chosen here to demonstrate the concept. In real scenarios, the equilibrium distribution may differ from log-normal and one would then require a different mapping (see, for example, appendix A). However, the details of the mapping from χ to V are irrelevant for the concept which is the focus of this paper.

3. JPDF transport equation

In this section, we present a mathematical framework that allows us to describe the stochastic models presented in § 2 in terms of a JPDF evolution. The concepts of JPDF and mass density functions (MDF) in the context of multi-phase flow are introduced and their evolution equations are derived from the stochastic models presented above. The stochastic processes considered in the present work are $\boldsymbol{X}(t) = \{X_1(t), X_2(t), X_3(t)\}^{\mathrm{T}}$, $V(t)$, $N(t)$ and $A(t)$. While the processes $\boldsymbol{X}(t)$ and $V(t)$

are continuous, $N(t)$ is a jump process with binary states and $A(t)$ does not vary in time. If $\mathscr{G}(\boldsymbol{x}, v, n, a; t)$ is the JPDF of $\boldsymbol{X}(t)$, $V(t)$, $N(t)$ and $A(t)$ defined in the probability space $\boldsymbol{x}$–v–n–a, then the probability of finding at time t an infinitesimal fluid element in a phase-a ganglion of size $V(t) \in [v, v + \mathrm{d}v]$ in state n located at $X(t) \in [\boldsymbol{x}, \boldsymbol{x} + \mathrm{d}\boldsymbol{x}]$ is given by $\mathscr{G}(\boldsymbol{x}, v, n, a; t)\,\mathrm{d}x_1\,\mathrm{d}x_2\,\mathrm{d}x_3\,\mathrm{d}v$. An obvious constraint of the above definition is the normalization condition

$$\sum_{(a,n)\in\mathbb{I}^2} \int_{\mathbb{R}^4} \mathscr{G}(\boldsymbol{x}, v, n, a; t)\,\mathrm{d}v\,\mathrm{d}x_1\,\mathrm{d}x_2\,\mathrm{d}x_3 \equiv 1, \tag{3.1}$$

where $\mathbb{I}$ denotes the set of all integers and $\mathbb{R}$ the set of all real numbers. The evolution of $\mathscr{G}(\boldsymbol{x}, v, n, a; t)$ is governed by the DCKE (Gardiner 2004)

$$\begin{aligned}\frac{\partial \mathscr{G}}{\partial t} + \frac{\partial}{\partial x_i}\{D^{x_i}\mathscr{G}\} + \frac{\partial}{\partial v}\{D^{v}\mathscr{G}\} = \frac{\partial^2}{\partial x_i \partial x_j}\{D^{x_i,x_j}\mathscr{G}\} + \frac{\partial^2}{\partial v \partial v}\{D^{v,v}\mathscr{G}\} + \frac{\partial^2}{\partial x_i \partial v}\{D^{x_i,v}\mathscr{G}\} \\ + \sum_{m\in\mathbb{I}^1}[T(n \mid m; \boldsymbol{x}, v, a, t)\mathscr{G}(\boldsymbol{x}, v, m, a; t) - T(m \mid n; \boldsymbol{x}, v, a, t)\mathscr{G}(\boldsymbol{x}, v, n, a; t)],\end{aligned} \tag{3.2}$$

which is a parabolic partial differential equation (PDE) for $\mathscr{G}$ with a source term. The first term on the left-hand side represents accumulation of $\mathscr{G}$ and the next two terms describe convection in physical and ganglion size spaces, where the coefficients D^{x_i} and D^{v} are obtained as

$$D^{x_i} = \lim_{\Delta t\to 0} \frac{1}{\Delta t}\langle X_i(t + \Delta t) - X_i(t) \mid \boldsymbol{x}, v, n, a; t\rangle \tag{3.3a}$$

and

$$D^{v} = \lim_{\Delta t\to 0} \frac{1}{\Delta t}\langle V(t + \Delta t) - V(t) \mid \boldsymbol{x}, v, n, a; t\rangle. \tag{3.3b}$$

The first two terms on the right-hand side of (3.2) account for diffusion in physical and ganglion size spaces, and the third describes cross-diffusion between these two spaces. The corresponding diffusion coefficients are obtained as

$$D^{x_i,x_j} = \lim_{\Delta t\to 0} \frac{1}{2\Delta t}\langle\{X_i(t + \Delta t) - X_i(t)\}\{X_j(t + \Delta t) - X_j(t)\} \mid \boldsymbol{x}, v, n, a; t\rangle, \tag{3.4a}$$

$$D^{v,v} = \lim_{\Delta t\to 0} \frac{1}{2\Delta t}\langle\{V(t + \Delta t) - V(t)\}\{V(t + \Delta t) - V(t)\} \mid \boldsymbol{x}, v, n, a; t\rangle \tag{3.4b}$$

and

$$D^{x_i,v} = \lim_{\Delta t\to 0} \frac{1}{2\Delta t}\langle\{X_i(t + \Delta t) - X_i(t)\}\{V(t + \Delta t) - V(t)\} \mid \boldsymbol{x}, v, n, a; t\rangle. \tag{3.4c}$$

The last term of (3.2) accounts for the jump process $N(t)$ with the jump rate

$$T(n \mid m; \boldsymbol{x}, v, a, t) = \lim_{\Delta t\to 0} \frac{P(n, t + \Delta t \mid m; \boldsymbol{x}, v, a, t)}{\Delta t}, \tag{3.5}$$

where $P(n, t + \Delta t \mid m; \boldsymbol{x}, v, a, t)$ is the probability at time t for $N(t)$ to jump from the state $(\boldsymbol{x}, v, m, a)$ to $(\boldsymbol{x}, v, n, a)$ in the time interval Δt. It is worthwhile to mention two important special cases of (3.2). One is the Fokker–Planck equation, if no jump process exists, and the other is the Master equation, if only jump processes exist.

3.1. *Mass density function (MDF)*

While dealing with non-uniform density or multi-phase flows the formulation based on MDFs has a number of advantages over the one based on JPDFs (Pope 1985). The MDF $\mathscr{F}(\boldsymbol{x}, v, n, a; t)$ of $\boldsymbol{X}(t)$, $V(t)$, $N(t)$ and $A(t)$ is defined in the space $\boldsymbol{x}$–v–n–a, such that at time t the expected mass of phase-a ganglia of size $V(t) \in [v, v + \mathrm{d}v]$ in state n with $X(t) \in [\boldsymbol{x}, \boldsymbol{x}+\mathrm{d}\boldsymbol{x}]$ is $\mathscr{F}(\boldsymbol{x}, v, n, a; t)\,\mathrm{d}x_1\,\mathrm{d}x_2\,\mathrm{d}x_3\,\mathrm{d}v$. One can easily show that $\mathscr{F}(\boldsymbol{x}, v, n, a; t) = \mathscr{M}\mathscr{G}(\boldsymbol{x}, v, n, a; t)$, where $\mathscr{M}$ is the total fluid mass in the domain. Note that here $\mathscr{G}$ is assumed to be a mass-weighted JPDF. The MDF has the important property that

$$\sum_{n\in\mathbb{I}^1}\int_{\mathbb{R}^1}\mathscr{F}(\boldsymbol{x}, v, n, a; t)\,\mathrm{d}v = \phi\rho_a S_a, \tag{3.6}$$

where ρ_a and S_a are the mean phase density and saturation of phase a. In this paper, we assume that the phase densities are constant.

3.2. *Modelled MDF-transport equation*

The coefficients (3.3)–(3.5) in (3.2) are evaluated using the stochastic models presented in § 2. The mathematical details of evaluating the stochastic limits involved can be found in the standard textbooks on stochastic methods (see Gardiner 2004, for example); below only the final expressions are given:

$$D^{x_i} = u_i = -n\frac{k_{r_a}k}{\phi S_a\mu_a}\left(\frac{\partial p_a}{\partial x_i} + \rho_a g e_{z_i}\right), \quad D^{v} = -\frac{v}{\tau_v}\left(\log\frac{v}{V^{eq}} - \frac{\sigma^2}{2}\right), \tag{3.7}$$

$$D^{x_i,x_j} = \begin{cases} 2\Gamma|\boldsymbol{u}| & \text{if } i = j \\ 0 & \text{if } i \neq j, \end{cases} \quad D^{v,v} = \frac{v^2\sigma^2}{\tau_v}, \quad D^{x_i,v} = 0, \tag{3.8}$$

and

$$T(n \mid m; \boldsymbol{x}, v, a, t) = \delta_{m0}\delta_{n1}\alpha_M + \delta_{m1}\delta_{n0}\alpha_T. \tag{3.9}$$

Substitution of the expressions (3.7)–(3.9) and $\mathscr{G} = \mathscr{F}/\mathscr{M}$ into (3.2) leads to the modelled MDF-transport equation

$$\begin{aligned}
&\frac{\partial\mathscr{F}}{\partial t} + \frac{\partial}{\partial x_i}\left\{-n\frac{k_{r_a}k}{\phi S_a\mu_a}\left(\frac{\partial p_a}{\partial x_i} + \rho_a g e_{z_i}\right)\mathscr{F}\right\} + \frac{\partial}{\partial v}\left\{-\frac{v}{\tau_v}\left(\log\frac{v}{V^{eq}} - \frac{\sigma^2}{2}\right)\mathscr{F}\right\} \\
&\quad = \frac{\partial^2}{\partial x_i\partial x_i}\{\Gamma|\boldsymbol{u}|\mathscr{F}\} + \frac{\partial^2}{\partial v^2}\left\{\frac{v^2\sigma^2}{\tau_v}\mathscr{F}\right\} \\
&\qquad + \sum_{m=\mathbb{I}^1}(\delta_{m0}\delta_{n1}\alpha_M + \delta_{m1}\delta_{n0}\alpha_T)\mathscr{F}(\boldsymbol{x}, v, m, a; t) \\
&\qquad - \sum_{m=\mathbb{I}^1}(\delta_{n0}\delta_{m1}\alpha_M + \delta_{n1}\delta_{m0}\alpha_T)\mathscr{F}(\boldsymbol{x}, v, n, a; t).
\end{aligned} \tag{3.10}$$

Once the required model parameters are provided, (3.10) fully describes the flow for a given set of initial and boundary conditions. In principle, deterministic methods such as finite volume or finite element schemes can be employed to solve the MDF equation; however, owing to its high-dimensionality this is computationally expensive. An alternative approach to solve (3.10) is based on evolving Lagrangian particles by the stochastic rules presented in § 2 and extracting the required statistics from particle ensembles. A detailed description of this strategy can be found in Tyagi *et al.* (2008).

3.3. *Moment transport equations*

An MDF contains the complete one-point one-time statistics of the variables defining the probability space. Therefore, (3.10) can be used to derive transport equations for stochastic moments such as expectations, variances, covariances etc. To explain how this can be done in general, let $Q(V,N)$ be some function of V and N. Its mass-weighted phase average (Favre average) can be evaluated as (see e.g. Pope 1985; Naud 2003, for the detailed derivation)

$$\sum_{n\in\mathbb{I}^1}\int_{\mathbb{R}^1} Q(v,n)\mathscr{F}(\boldsymbol{x},v,n,a;t)\,\mathrm{d}v=\phi\rho_a(\boldsymbol{x},t)S_a(\boldsymbol{x},t)\overline{Q(V,N)\mid a,\boldsymbol{x}}(t). \tag{3.11}$$

A transport equation for $\overline{Q(V,N)\mid a,\boldsymbol{x}}$ in physical space can be derived by multiplying (3.10) with $Q(v,n)$ and subsequently applying the operator $\sum_{n\in\mathbb{I}^1}\int_{\mathbb{R}^1}\mathrm{d}v$. With $Q(v,n)=1$ one obtains the continuity equation for phase a, i.e.

$$\frac{\partial}{\partial t}(\phi\rho_a S_a)-\boldsymbol{\nabla}\cdot\left\{\overline{N\mid a,\boldsymbol{x}}\frac{\rho_a k_{r_a}k}{\mu_a}(\boldsymbol{\nabla}p_a+\rho_a g\boldsymbol{e}_z)\right\}=\nabla^2(\phi\rho_a S_a\overline{\Gamma|\boldsymbol{U}|\mid a,\boldsymbol{x}}). \tag{3.12}$$

Notice that even if pore-scale dispersion is ignored, the convection term in (3.12) is unclosed since $\overline{N\mid a,\boldsymbol{x}}$ is an unknown quantity. In the traditional deterministic Darcy's-law-based formulation, one treats $\overline{N\mid a,\boldsymbol{x}}$ as a function of saturation, so that the effective relative permeability $\overline{N\mid a,\boldsymbol{x}}k_{r_a}$ also is a function of saturation (Bear 1972). However, in the present model $\overline{N\mid a,\boldsymbol{x}}$ is transported by

$$\begin{aligned}&\frac{\partial}{\partial t}(\phi\rho_a S_a\overline{N\mid a,\boldsymbol{x}})-\boldsymbol{\nabla}\cdot\left\{\overline{N\mid a,\boldsymbol{x}}\frac{\rho_a k_{r_a}k}{\mu_a}(\boldsymbol{\nabla}p_a+\rho_a g\boldsymbol{e}_z)\right\}\\&\quad=\nabla^2(\phi\rho_a S_a\overline{\Gamma|\boldsymbol{U}|N\mid a,\boldsymbol{x}})+\phi\rho_a S_a\{\overline{\alpha_M\mid a,\boldsymbol{x}}-(\overline{\alpha_M N\mid a,\boldsymbol{x}}+\overline{\alpha_T N\mid a,\boldsymbol{x}})\},\end{aligned} \tag{3.13}$$

which is obtained by choosing $Q(v,n)=n$. While convection in (3.13) is closed, pore-scale dispersion requires modelling. In general, also the source term is unclosed, if α_M and α_T are functions of ganglion size. In that case, closure of the source term requires higher joint moments of V and N. Transport of the mean ganglion size $\overline{V\mid a,\boldsymbol{x}}$ is governed by

$$\begin{aligned}&\frac{\partial}{\partial t}(\phi\rho_a S_a\overline{V\mid a,\boldsymbol{x}})-\boldsymbol{\nabla}\cdot\left\{\overline{VN\mid a,\boldsymbol{x}}\frac{\rho_a k_{r_a}k}{\mu_a}(\boldsymbol{\nabla}p_a+\rho_a g\boldsymbol{e}_z)\right\}\\&\quad=\nabla^2(\phi\rho_a S_a\overline{\Gamma|\boldsymbol{U}|V\mid a,\boldsymbol{x}})-\frac{\phi\rho_a S_a}{\tau_v}\left\{\overline{V\log\left(\frac{V}{V^{eq}}\right)\middle|a,\boldsymbol{x}}-\overline{\frac{V\sigma^2}{2}\middle|a,\boldsymbol{x}}\right\},\end{aligned} \tag{3.14}$$

which is obtained by choosing $Q(v,n)=v$. Closing (3.14) requires higher moments and so the higher-moment transport equations, which leads to a closure problem, unless the full JPDF is known. Therefore, with a system of a finite number of moment equations it is in general not possible to achieve closure. On the other hand, no such closure problems arise if the MDF-equation (3.10) is solved.

The closure problem that arises while averaging a micro-scale flow description is essentially due to the inherent nonlinear behaviour of the micro-scale flow dynamics. In such scenarios, if fluctuations and correlations cannot be ignored, average quantities alone are not sufficient to describe the average flow behaviour (at the macro-scale). Ganglia mobilization, trapping, coalescence and breakup are highly nonlinear pore-scale phenomena, typically leading to closure problems. Here it is worthwhile to

mention that similar closure problems are encountered in other areas of fluid dynamics; for example in modelling turbulent flows (Pope 1985). It will be shown in § 3.5 that the flow in question has several time scales, which essentially signify the presence of various correlations in the flow. Closure may only be obtained if correlation times are very short; some scenarios of this kind, for which closure can be achieved with a finite number of moment equations, are presented in §§ 4 and 5. It is emphasized, however, that a proper time scale analysis is required to justify the applicability of such a simplified model. In the general case such simplifications cannot be made, but note that the SPM can be employed in any case, even if closure cannot be obtained with a finite number of moment equations.

3.4. *Pressure equation*

An equation for the pressure p_1, which is a deterministic Eulerian variable (function of $\boldsymbol{x}$ and t), follows from mass conservation. To derive the pressure equation we apply the operator $\sum_{a\in\mathbb{I}^1}$ to (3.12), which leads to

$$-\boldsymbol{\nabla}\cdot\left\{k\sum_{a\in\mathbb{I}^1}\left(\overline{N\mid a,\boldsymbol{x}}\frac{\rho_a k_{r_a}}{\mu_a}\left(\boldsymbol{\nabla}p_a+\rho_a g\boldsymbol{e}_z\right)\right)\right\}$$
$$=-\frac{\partial}{\partial t}\sum_{a\in\mathbb{I}^1}(\phi\rho_a S_a)+\nabla^2\left\{\phi\sum_{a\in\mathbb{I}^1}\left(\rho_a S_a\overline{\Gamma|\boldsymbol{U}|\mid a,\boldsymbol{x}}\right)\right\}. \tag{3.15}$$

This is the total mass balance of all phases at any point $\boldsymbol{x}$ and time t. Substitution of p_a using the relationship $p_a = p_1 - \sum_{b=1}^{a-1} p_{c_b}$, where p_{c_b} is the macroscopic capillary pressure between the phases b and $b+1$ (see Tyagi *et al.* 2008, for the detailed derivation), leads to

$$-\boldsymbol{\nabla}\cdot\left\{k\sum_{a\in\mathbb{I}^1}\left(\overline{N\mid a,\boldsymbol{x}}\frac{\rho_a k_{r_a}}{\mu_a}\right)\boldsymbol{\nabla}p_1\right\}=\boldsymbol{\nabla}\cdot\left\{k\sum_{a\in\mathbb{I}^1}\left(\overline{N\mid a,\boldsymbol{x}}\frac{\rho_a k_{r_a}}{\mu_a}\rho_a g\boldsymbol{e}_z\right)\right\}$$
$$-\boldsymbol{\nabla}\cdot\left\{k\sum_{a\in\mathbb{I}^1}\left(\overline{N\mid a,\boldsymbol{x}}\frac{\rho_a k_{r_a}}{\mu_a}\sum_{b=1}^{a-1}\boldsymbol{\nabla}p_{c_b}\right)\right\}-\frac{\partial}{\partial t}\sum_{a\in\mathbb{I}^1}(\phi\rho_a S_a)$$
$$+\nabla^2\left\{\phi\sum_{a\in\mathbb{I}^1}\left(\rho_a S_a\overline{\Gamma|\boldsymbol{U}|\mid a,\boldsymbol{x}}\right)\right\}. \tag{3.16}$$

The first and second right-hand-side terms account for the influence of gravity and macroscopic capillary pressure, respectively. The third right-hand-side term represents compressibility effects due to density variations and the last term accounts for pore-scale dispersion (this is similar to the correction term in the particle displacement model introduced by Kinzelbach 1992).

3.5. *Time scales*

There exist various characteristic time scales associated with stochastic processes in the present model. Let U be the magnitude of a reference flow velocity and L a macroscopic characteristic length scale. Thus, convection and diffusion time scales can

be expressed as

$$\tau_x = \frac{L}{\phi U} \quad \text{and} \quad \tau_{xx} = \tau_x \frac{L}{\Gamma}, \tag{3.17}$$

respectively. Here we consider subsurface flow with $\Gamma \ll L$, and therefore τ_x becomes the characteristic time scale of the flow. For the dynamics in the v-space, the characteristic time scale is τ_v, which indicates how fast the distribution of $V(t)$ approaches the equilibrium distribution (log-normal in the case of constant τ_v and σ^2). The characteristic time scale for the dynamics in the n-space is

$$\tau_n = \frac{1}{\alpha_{M0} + \alpha_{T0}}, \tag{3.18}$$

where α_{M0} and α_{T0} are the reference mobilization and trapping rates. Again τ_n indicates how fast the distribution of $N(t)$ achieves equilibrium. In the following three sections, the asymptotic behaviour of (3.10) for $\tau_v \ll \tau_x \gg \tau_n$, $\tau_x \gg \tau_v \ll \tau_n$ and $\tau_x \gg \tau_n \ll \tau_v$ is investigated.

4. Quasi-uniform and very slow flow ($\tau_v \ll \tau_x \gg \tau_n$)

For spatially uniform or quasi-uniform (at the observation length scale) flow, the models can be greatly simplified, thus allowing us to gain better understanding of the ganglion dynamics (i.e the dynamics of $N(t)$ and $V(t)$ together). Moreover, the special case of very slow flow is closely related to quasi-uniform flow. Here, we consider cases with $\tau_v \ll \tau_x \gg \tau_n$ and for further clarification we investigate the behaviour of (3.10) for slow and fast dimensionless times, i.e. $t_s = t/\tau_x$ and $t_f = t/\tau_n$, respectively. For the slow time, an 'outer' solution of (3.10) approximates very slow flows where only the stationary joint distribution of $N(t)$ and $V(t)$ is required to close the model. In the theory of stochastic processes, such an approximation is known as adiabatic elimination of fast variables (Gardiner 2004). For the fast time, an 'inner' solution of (3.10) is obtained that approximates quasi-uniform flows. The stationary distribution of $V(t)$ and $N(t)$ obtained from the inner solution is indeed the one required to close the outer solution.

At this point, we must mention that though a log-normal ganglion size process described by (2.10) is used in the following development and also in § 5, the final results are general and valid for all continuous ganglion size processes which can be described by (2.7) and have the autocorrelation time τ_v. For example, one can also derive same results using a Gamma process (A 15); this is done in appendix A to compare results with the birth–death approach.

4.1. *Outer solution for t_s*

Scaling the time in (3.10) with τ_x and then taking the limits $\tau_v/\tau_x \to 0$ and $\tau_n/\tau_x \to 0$ leads to

$$-\frac{\partial}{\partial \eta}\left\{\frac{\eta}{\tau_v}\mathscr{G}(\boldsymbol{x}, \eta, n=0, a; t_s)\right\} = \frac{\partial^2}{\partial \eta^2}\left\{\frac{\sigma^2}{\tau_v}\mathscr{G}(\boldsymbol{x}, \eta, n=0, a; t_s)\right\} + \alpha_T \mathscr{G}(\boldsymbol{x}, \eta, n=1, a; t_s) - \alpha_M \mathscr{G}(\boldsymbol{x}, \eta, n=0, a; t_s) \tag{4.1a}$$

and

$$-\frac{\partial}{\partial \eta}\left\{\frac{\eta}{\tau_v}\mathscr{G}(\boldsymbol{x}, \eta, n=1, a; t_s)\right\} = \frac{\partial^2}{\partial \eta^2}\left\{\frac{\sigma^2}{\tau_v}\mathscr{G}(\boldsymbol{x}, \eta, n=1, a; t_s)\right\} + \alpha_M \mathscr{G}(\boldsymbol{x}, \eta, n=0, a; t_s) - \alpha_T \mathscr{G}(\boldsymbol{x}, \eta, n=1, a; t_s), \tag{4.1b}$$

for the JPDF $\mathscr{G}(\boldsymbol{x}, \eta, n, a; t)$, where η is the sample space variable of χ and $v = V^{eq}\exp(\eta - \sigma^2/2)$. Equations (4.1*a*) and (4.1*b*) are two coupled linear ordinary differential equations (ODEs) and their general solution with the boundary conditions $\mathscr{G}(\boldsymbol{x}, \eta \to \pm\infty, n, a; t_s) = \partial_\eta \mathscr{G}(\boldsymbol{x}, \eta \to \pm\infty, n, a; t_s) = 0$ can be written as $\mathscr{G}(\boldsymbol{x}, \eta, n, a; t_s) = \mathscr{H}(\boldsymbol{x}, a; t_s)\,\mathscr{J}(\eta, n; \boldsymbol{x}, a, t_s)$, where $\mathscr{H}$ is an arbitrary function of $\boldsymbol{x}$, a and t_s, and $\mathscr{J}$ a known quasi-stationary JPDF of $N(t)$ and $\chi(t)$ with $\boldsymbol{x}$, a and t_s as parameters. Comparing this solution with the identity

$$\mathscr{G}(\boldsymbol{x}, \eta, n, a; t_s) = \mathscr{G}(\eta, n \mid \boldsymbol{x}, a; t_s)\mathscr{G}(\boldsymbol{x}, a; t_s) \tag{4.2}$$

gives $\mathscr{G}(\eta, n \mid \boldsymbol{x}, a; t_s) = \mathscr{J}(\eta, n; \boldsymbol{x}, a, t_s)$ and $\mathscr{G}(\boldsymbol{x}, a; t) = \mathscr{H}(\boldsymbol{x}, a; t_s)$. This decoupling of the JPDF leads to the closure of the term $\overline{N \mid a, \boldsymbol{x}}$ in (3.12), since one can write

$$\begin{aligned}\mathscr{M}\sum_{n\in\mathbb{I}^1} n\int_{\mathbb{R}^1}\mathscr{G}(\boldsymbol{x}, \eta, n, a; t_s)\,\mathrm{d}\eta &= \sum_{n\in\mathbb{I}^1} n\int_{\mathbb{R}^1}\mathscr{G}(\eta, n \mid \boldsymbol{x}, a; t_s)\,\mathrm{d}\eta\,\mathscr{M}\mathscr{G}(\boldsymbol{x}, a; t_s)\\ &= \underbrace{\sum_{n\in\mathbb{I}^1} n\int_{\mathbb{R}^1}\mathscr{J}(\eta, n; \boldsymbol{x}, a, t_s)\,\mathrm{d}\eta}_{\equiv\varsigma(\boldsymbol{x}, a, t_s)}\ \underbrace{\mathscr{M}\mathscr{H}(\boldsymbol{x}, a; t_s)}_{\equiv\mathscr{F}(\boldsymbol{x}, a; t_s)}\end{aligned} \tag{4.3}$$

from which follows that

$$\overline{N \mid a, \boldsymbol{x}}(t_s) = \varsigma(\boldsymbol{x}, a, t_s)\mathscr{F}(\boldsymbol{x}, a; t_s)/(\phi(\boldsymbol{x})\rho_a(\boldsymbol{x}, t_s)S_a(\boldsymbol{x}, t_s)) = \varsigma(\boldsymbol{x}, a, t_s). \tag{4.4}$$

Since ς is a known function of $\boldsymbol{x}$, a and t_s, the phase-a continuity equation (3.12) (for $\Gamma = 0$)

$$\frac{\partial}{\partial t}(\phi\rho_a S_a) - \boldsymbol{\nabla}\cdot\left\{\varsigma\frac{\rho_a k_{r_a} k}{\mu_a}(\boldsymbol{\nabla}p_a + \rho_a g\boldsymbol{e}_z)\right\} = 0, \tag{4.5}$$

is closed. A specific form of the function ς depends on τ_v, σ^2, α_M and α_T, which are macroscopic statistical parameters. In (4.5), the effective relative permeability is $k^e_{r_a} = \varsigma k_{r_a}$ and if ς is only a function of saturation, the traditional equilibrium model is recovered. The effect of pore-scale processes on the effective relative permeability is via τ_v, σ^2, α_M and α_T, which is investigated in the following section.

4.2. *Inner solution for t_f*

Here, ganglion dynamics is studied in a spatially uniform flow by investigating the inner solution of (3.10) on the fast time t_f. Scaling the time in (3.10) with τ_n and then taking the limit $\tau_n/\tau_x \to 0$ leads to a set of two linear PDEs (one for $n = 0$ and one for $n = 1$) for the JPDF $f(\eta, n; t)$ of $\chi(t)$ and $N(t)$ in η–n-space, i.e.

$$\begin{aligned}\frac{\partial f(\eta, 0; t)}{\partial t} - \frac{\partial}{\partial\eta}\left\{\frac{\eta}{\tau_v}f(\eta, 0; t)\right\} &= \frac{\partial^2}{\partial\eta\partial\eta}\left\{\frac{\sigma^2}{\tau_v}f(\eta, 0; t)\right\}\\ &\quad + \alpha_T f(\eta, 1; t) - \alpha_M f(\eta, 0; t)\end{aligned} \tag{4.6a}$$

and

$$\begin{aligned}\frac{\partial f(\eta, 1; t)}{\partial t} - \frac{\partial}{\partial\eta}\left\{\frac{\eta}{\tau_v}f(\eta, 1; t)\right\} &= \frac{\partial^2}{\partial\eta\partial\eta}\left\{\frac{\sigma^2}{\tau_v}f(\eta, 1; t)\right\}\\ &\quad + \alpha_M f(\eta, 0; t) - \alpha_T f(\eta, 1; t).\end{aligned} \tag{4.6b}$$

Equations (4.6*a*) and (4.6*b*) must be solved simultaneously for $f(\eta, n; t)$, which can then be used to find the desired stochastic moments. Next, some interesting cases are

investigated that arise from the coupling between $N(t)$ and $V(t)$. In all cases discussed below, the stationary mean of $N(t)$ is equal to the macroscopic parameter ς appearing in (4.5), i.e.

$$\varsigma = \lim_{t_f \to \infty} \overline{N(\tau_n t_f)} = \overline{N}_\infty. \tag{4.7}$$

In general, the actual dependence of α_M and α_T on v can be determined from pore-scale simulation studies or experiments, for example from the work of Dias & Payatakes (1986*b*), where probabilities of mobilization and trapping as functions of the ganglion size are provided. In appendix A, we derive expressions for these rates as functions of the quantities that appear in the birth–death population balance model (Valavanides *et al.* 1998).

4.2.1. *No coupling*

First, the simplest case, in which the ganglion mobilization and trapping events are independent of the ganglion coalescence and breakup, is considered. $N(t)$ is then a pure jump process with constant mobilization and trapping rates, i.e. $\alpha_M = \alpha_{M0}$ and $\alpha_T = \alpha_{T0}$, which is also known as the random telegraph process due to its first use in modelling binary telegraph signals (Gardiner 2004). Since $V(t)$ and $N(t)$ are independent, (4.6*a*) and (4.6*b*) can be integrated over η-space to obtain

$$\frac{\mathrm{d}f(0)}{\mathrm{d}t} = \alpha_{T0} f(1) - \alpha_{M0} f(0) \quad \text{and} \quad \frac{\mathrm{d}f(1)}{\mathrm{d}t} = \alpha_{M0} f(0) - \alpha_{T0} f(1) \tag{4.8}$$

for the PDF of $N(t)$. These are two Master equations for $f(n)$, which is a bimodal PDF with peaks at $n = 0$ (trapped state) and $n = 1$ (mobile state) of amplitudes $f(0)$ and $f(1)$, respectively. Equation (4.8) is a set of two coupled linear ODEs with constant coefficients and can be solved analytically. Their statistically stationary solution is

$$f_\infty(n) = \delta_{n0} \frac{\alpha_{T0}}{\alpha_{M0} + \alpha_{T0}} + \delta_{n1} \frac{\alpha_{M0}}{\alpha_{M0} + \alpha_{T0}}, \tag{4.9}$$

which can be used to find the mean and variance of $N(t)$, i.e.

$$\overline{N(t)}_\infty = \frac{\alpha_{M0}}{\alpha_{M0} + \alpha_{T0}}, \quad \mathrm{var}\{N(t)\}_\infty = \frac{\alpha_{M0}\alpha_{T0}}{(\alpha_{M0} + \alpha_{T0})^2}. \tag{4.10}$$

The stationary autocorrelation function of the system is

$$R(s)_\infty = \exp[-(\alpha_{M0} + \alpha_{T0})s], \tag{4.11}$$

where $\tau_n = 1/(\alpha_{M0} + \alpha_{T0})$ is the autocorrelation time, which is same as the characteristic time scale of the process $N(t)$ defined in § 3.5 (3.18).

This simple case shows how the ganglion mobilization and trapping affect the average phase velocity. Given α_{M0} and α_{T0} as functions of saturation, one obtains the effective permeability, which can be used in the multiphase Darcy formulation. Note that ς remains bounded between 0 and 1 irrespective of the values of α_{M0} and α_{T0}.

4.2.2. *Subinner solution ($\tau_v \ll \tau_n$)*

If the coalescence and breakup rates are much higher than the mobilization and trapping rates, (4.6*a*) and (4.6*b*) can be simplified by eliminating the η-dependent terms. However, this elimination of η is different from the one performed in § 4.2.1 as here no assumption about the nature of the coupling is made. Taking the limits

$\tau_v/\tau_n \to 0$ in (4.6*a*) and (4.6*b*), and subsequently integrating leads to

$$f(\eta; n) = f(\eta \mid n) = \frac{1}{\sqrt{2\pi\sigma^2(n)}} \exp\left\{-\frac{\eta^2}{2\sigma^2(n)}\right\} \tag{4.12}$$

for $\tau_f \gg \tau_v$, where σ^2 is assumed to be independent of η (although this can be relaxed for a more general analysis). Substitution of $f(\eta, n) = f(\eta; n)f(n)$ in (4.6*a*) and (4.6*b*) and subsequent integration over η-space gives

$$\left.\begin{aligned} \frac{\mathrm{d}f(n=0)}{\mathrm{d}t} &= \beta_T f(n=1) - \beta_M f(n=0), \\ \frac{\mathrm{d}f(n=1)}{\mathrm{d}t} &= \beta_M f(n=1) - \beta_T f(n=1), \end{aligned}\right\} \tag{4.13}$$

where β_M and β_T are the average mobilization and trapping rates and are defined by

$$\beta_M = \int_{\mathbb{R}^1} \alpha_M(\eta) f(\eta; 0)\,\mathrm{d}\eta \quad \text{and} \quad \beta_T = \int_{\mathbb{R}^1} \alpha_T(\eta) f(\eta; 1)\,\mathrm{d}\eta. \tag{4.14}$$

Notice that only the stationary distribution of $\chi(t)$, i.e. mean and variance, is required to describe the ganglia motion. The rest of the analysis is the same as performed in § 4.2.1 with α_{M0} and α_{T0} in (4.8) replaced by β_M and β_T, respectively. It is interesting to note that if α_M and α_T are nonlinear functions of v, it is not only the mean, but also the variance of $V(t)$ that influences $N(t)$. This is characteristic for stochastic system with microscopic nonlinearity.

5. Rapid ganglion coalescence and breakup ($\tau_n \gg \tau_v \ll \tau_x$)

This section investigates the important limiting case in which ganglion coalescence and breakup occur much more rapidly than convection, mobilization and trapping. This would lead to a stochastic system in which the distribution of $V(t)$ is quasi-stationary. The same idea was exploited in § 4 to eliminate fast variables. Scaling the time in (3.10) with τ_x and subsequently taking the limits $\tau_v/\tau_x \to 0$ and $\tau_v/\tau_n \to 0$ yields

$$\frac{\partial}{\partial\eta}\left\{-\frac{\eta}{\tau_v}\mathscr{G}\right\} = \frac{\partial^2}{\partial\eta\partial\eta}\left\{\frac{\sigma^2}{\tau_v}\mathscr{G}\right\} \tag{5.1}$$

for the JPDF $\mathscr{G}(\boldsymbol{x}, \eta, n, a; t)$ in η-space, where the transformation $v = V^{eq}\exp(\eta - \sigma^2/2)$ is used. Since (5.1) is a linear ODE, it can easily be solved by integrating it twice. Its solution satisfying the boundary conditions $\mathscr{G}(\eta \to \infty) = \mathscr{G}(\eta \to -\infty) = \partial_\eta\mathscr{G}(\eta \to \infty) = \partial_\eta\mathscr{G}(\eta \to -\infty) = 0$ is

$$\mathscr{G}(\boldsymbol{x}, \eta, n, a; t) = \mathscr{H}(\boldsymbol{x}, n, a; t)\exp\left(-\int_{\mathbb{R}^1}\frac{\eta}{2\sigma^2}\,\mathrm{d}\eta\right), \tag{5.2}$$

where $\mathscr{H}$ is an arbitrary function of $\boldsymbol{x}, n, a$ and t. Note that no specific assumptions about the parameters τ_v, σ^2 and V^{eq} are required to derive (5.2). In general, they can depend on $\boldsymbol{x}, n, a, \eta$ and t. Comparing

$$\mathscr{G}(\boldsymbol{x}, \eta, n, a; t) = \mathscr{G}(\eta \mid \boldsymbol{x}, n, a; t)\mathscr{G}(\boldsymbol{x}, n, a; t) \tag{5.3}$$

with (5.2) gives $\mathscr{G}(\boldsymbol{x}, n, a; t) = \mathscr{H}(\boldsymbol{x}, n, a; t)$ and $\mathscr{G}(\eta \mid \boldsymbol{x}, n, a; t) = \exp(-\int_{\mathbb{R}^1}\eta/(2\sigma^2)\,\mathrm{d}\eta)$, where the latter is a known function.

Next, similar to § 4, we show that the decomposition (5.3) of the JPDF leads to a closure of the source terms in (3.13). To this end, we first consider

$$\sum_{n\in\mathbb{I}^1} n \int_{\mathbb{R}^1} \alpha_M(\eta)\mathscr{G}(\boldsymbol{x},\eta,n,a;t)\,\mathrm{d}\eta = \sum_{n\in\mathbb{I}^1} n \underbrace{\int_{\mathbb{R}^1} \alpha_M(\eta)\mathscr{G}(\eta\mid\boldsymbol{x},n,a,t)\,\mathrm{d}\eta}_{=\beta_M(\boldsymbol{x},n,a,t)} \mathscr{G}(\boldsymbol{x},n,a;t) \tag{5.4}$$

from which follows that

$$\phi(\boldsymbol{x})\rho_a(\boldsymbol{x},t)S_a(\boldsymbol{x},t)\overline{\alpha_M(\eta)N\mid a,\boldsymbol{x}}(t) = \sum_{n\in\mathbb{I}^1} n\beta_M(\boldsymbol{x},n,a,t)\mathscr{F}(\boldsymbol{x},n,a;t), \tag{5.5}$$

where β_M is the average (conditioned on $\boldsymbol{x}$, n and a) mobilization rate. Since N is a binary random variable, β_M can be split as

$$\beta_M(\boldsymbol{x},n,a,t) = \beta_{M0}(\boldsymbol{x},a,t)\delta_{n0} + \beta_{M1}(\boldsymbol{x},a,t)\delta_{n1}, \tag{5.6}$$

where β_{M0} and β_{M1} are the conditional average mobilization rates of trapped and mobile ganglia, respectively. Note that β_{M1} does not have a physical meaning; it is only used here in the following derivation. For brevity we will omit writing the functional dependence in the following development, e.g. $\mathscr{F}(\boldsymbol{x},n,a;t)$ will be simply written as $\mathscr{F}$. Substitution of (5.6) into (5.5) gives

$$\phi\rho_a S_a\overline{\alpha_M N\mid a,\boldsymbol{x}} = \underbrace{\sum_{n\in\mathbb{I}^1} n\beta_{M0}\delta_{n0}\mathscr{F}}_{\equiv 0} + \sum_{n\in\mathbb{I}^1} n\beta_{M1}\delta_{n1}\mathscr{F} = \beta_{M1}\sum_{n\in\mathbb{I}^1} n\delta_{n1}\mathscr{F} \tag{5.7}$$

and since $n\delta_{n1} = n$, the above equation can be written as

$$\phi\rho_a S_a\overline{\alpha_M N\mid a,\boldsymbol{x}} = \beta_{M1}\underbrace{\sum_{n\in\mathbb{I}^1} n\mathscr{F}}_{\equiv\phi\rho_a S_a\overline{N\mid a,\boldsymbol{x}}}, \tag{5.8}$$

which leads to

$$\overline{\alpha_M N\mid a,\boldsymbol{x}} = \beta_{M1}\overline{N\mid a,\boldsymbol{x}}. \tag{5.9}$$

In a similar fashion, it can be shown that

$$\overline{\alpha_T N\mid a,\boldsymbol{x}} = \beta_{T1}\overline{N\mid a,\boldsymbol{x}}, \tag{5.10}$$

where β_{T1} is the conditional average trapping rate of mobile ganglia. Finally, $\overline{\alpha_M}$ can be evaluated as

$$\phi\rho_a S_a\overline{\alpha_M} = \sum_{n\in\mathbb{I}^1}\beta_{M0}\delta_{n0}\mathscr{F} + \sum_{n\in\mathbb{I}^1}\beta_{M1}\delta_{n1}\mathscr{F}. \tag{5.11}$$

Substituting $\delta_{n0} = 1-n$ and $\delta_{n1} = n$ in (5.11) leads to

$$\phi\rho_a S_a\overline{\alpha_M} = \beta_{M0}\underbrace{\sum_{n\in\mathbb{I}^1}(1-n)\mathscr{F}}_{\equiv\phi\rho_a S_a(1-\overline{N\mid a,\boldsymbol{x}})} + \beta_{M1}\underbrace{\sum_{n\in\mathbb{I}^1} n\mathscr{F}}_{\equiv\phi\rho_a S_a\overline{N\mid a,\boldsymbol{x}}}, \tag{5.12}$$

from which follows that

$$\overline{\alpha_M \mid a, \boldsymbol{x}} = \beta_{M0}(1 - \overline{N \mid a, \boldsymbol{x}}) + \beta_{M1}\overline{N \mid a, \boldsymbol{x}}. \tag{5.13}$$

Substitution of (5.9), (5.10) and (5.13) in (3.13) leads to (for $\Gamma = 0$)

$$\frac{\partial}{\partial t}(\phi\rho_a S_a \overline{N \mid a, \boldsymbol{x}}) - \boldsymbol{\nabla} \cdot \left\{ \overline{N \mid a, \boldsymbol{x}} \frac{\rho_a k_{ra} k}{\mu_a} (\boldsymbol{\nabla} p_a + \rho_a g \boldsymbol{e}_z) \right\}$$
$$= \phi\rho_a S_a \{\beta_{M0} - (\beta_{M0} + \beta_{T1})\overline{N \mid a, \boldsymbol{x}}\}, \tag{5.14}$$

which together with the continuity equation (3.12) (for $\Gamma = 0$)

$$\frac{\partial}{\partial t}(\phi\rho_a S_a) - \boldsymbol{\nabla} \cdot \left\{ \overline{N \mid a, \boldsymbol{x}} \frac{\rho_a k_{r_a} k}{\mu_a} (\boldsymbol{\nabla} p_a + \rho_a g \boldsymbol{e}_z) \right\} = 0 \tag{5.15}$$

forms a closed set of transport equations for the saturation S_a and the average mobility $\overline{N \mid a, \boldsymbol{x}}$. Since the convective fluxes in (5.14) and (5.15) are the same, subtracting them yields an equation without spatial derivatives, i.e.

$$\frac{\partial}{\partial t}\{\phi\rho_a S_a (1 - \overline{N \mid a, \boldsymbol{x}})\} = -\phi\rho_a S_a \{\beta_{M0} - (\beta_{M0} + \beta_{T1})\overline{N \mid a, \boldsymbol{x}}\}. \tag{5.16}$$

5.1. *Two-phase incompressible flow*

Consider incompressible two-phase flow of oil and water through an isotropic homogeneous porous medium (constant k and ϕ). Let S be the total oil saturation and $\zeta = S(1 - \overline{N \mid a = o})$ the trapped oil saturation, where $a = o$ indicates the oil phase. By defining the equilibrium trapped oil saturation $\zeta^{eq} = S\{1 - \beta_{M0}/(\beta_{M0} + \beta_{T1})\}$ and the average relaxation time $\overline{\tau}_\zeta = 1/(\beta_{M0} + \beta_{T1})$, (5.15) and (5.16) can be rewritten as

$$\phi \frac{\partial S}{\partial t} - \boldsymbol{\nabla} \cdot \left\{ \frac{(1 - \zeta/S) k_{r_o} k}{\mu_o} (\boldsymbol{\nabla} p_o + \rho_o g \boldsymbol{e}_z) \right\} = 0 \tag{5.17}$$

and

$$\frac{\partial \zeta}{\partial t} = -\frac{1}{\overline{\tau}_\zeta}(\zeta - \zeta^{eq}), \tag{5.18}$$

respectively. It is interesting to note that by considering the effect of pore-scale heterogeneity on the trapping process a very similar macroscopic model was also derived by Panfilov & Panfilova (1995). They argued that the time interval between successive appearances of traps can be significant; consequently, the average trapping process at macro-scale is governed by a kinetic equation. In appendix B, it is shown that for small $\overline{\tau}_\zeta$ the above two-equation model reduces to the non-equilibrium model proposed by Barenblatt *et al.* (2003), Silin & Patzek (2004) and Schembre & Kovscek (2006) and the well-known relative permeability–saturation hysteresis curves can naturally be obtained in this special case.

5.1.1. *Residual trapping*

This case corresponds to the limit of very small relaxation time $\overline{\tau}_\zeta$ in (5.18) and with the assumption that all ganglia are trapped, if $S < S_r$, but that no trapping occurs for $S \geqslant S_r$ (S_r denotes the residual saturation). In that case $\zeta = \zeta^{eq}$ with $\zeta^{eq} = S$, if $0 \leqslant S < S_r$ and $\zeta^{eq} = 0$, if $S_r \leqslant S \leqslant 1$. Note that this is equivalent to choosing $\varsigma = 1 - \zeta^{eq}/S$ in (4.5).

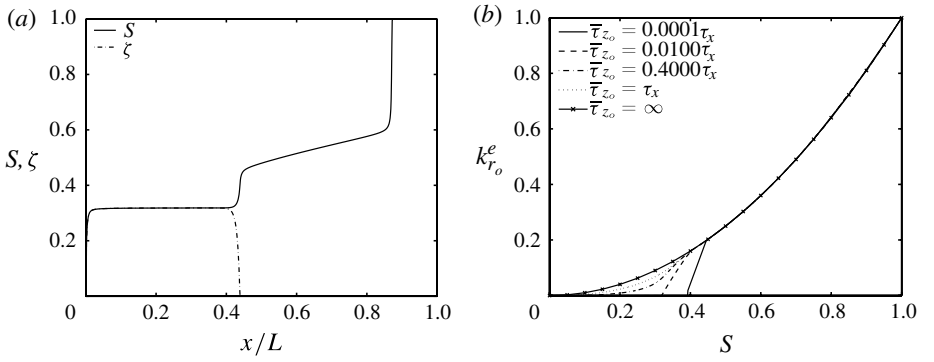

FIGURE 1. One-dimensional imbibition simulation results after the time $t = 0.5\tau_x$: (*a*) total oil saturation (S) and trapped oil saturation ζ for $\overline{\tau}_{z_o} = 10^{-2}\tau_x$; (*b*) effective relative permeability $k^e_{r_o} = (1 - \zeta/S)k_{r_o}$ curves for varying $\overline{\tau}_{z_o}$.

5.1.2. *Numerical results*

Equations (5.17) and (5.18) are numerically solved for a one-dimensional displacement problem with constant injection flux and in the absence of gravity. It is assumed that the oil phase remains connected if $S > S_c$, otherwise it exists in the form of disconnected ganglia. As the connected phase is always mobile, one obtains $\overline{\tau}_\zeta \to 0$ and $\zeta^{eq} = 0$ for $S > S_c$. While ganglion trapping is assumed to occur at a constant average rate $1/\overline{\tau}_{z_o}$, mobilization of the trapped ganglia (in the disconnected part of the phase) is ignored. This essentially implies that eventually all ganglia get trapped, hence $\zeta^{eq} = S$ for $S < S_c$. Depending on the saturation variation in a flow, trapped ganglia can become mobile again if they re-join the connected part of the phase. Such a flow scenario can, for example, be described by the following average mobilization and trapping rates:

$$\beta_{M0} = \begin{cases} 0 & \text{if } 0 < S < S_c \\ \\ 10^4/\tau_x & \text{if } S_c \leqslant S \leqslant 1, \end{cases} \qquad \beta_{T1} = \begin{cases} 1/\overline{\tau}_{z_o} & \text{if } 0 < S < S_c \\ \\ 0 & \text{if } S_c \leqslant S \leqslant 1, \end{cases} \tag{5.19}$$

where $S_c = 0.4$. Further, a quadratic oil relative permeability $k_{r_o} = S^2$ and a viscosity ratio of oil to water of 5 are chosen for the simulation. A finite volume method with first-order upwind scheme was employed to discretize the equations on an equally spaced grid with $\mathrm{d}x = 10^{-3}L$. The time integration was performed with a simple first-order Euler scheme and a time step size of $\mathrm{d}t = 10^{-6}\tau_x$ was chosen.

First, an imbibition process is considered in a domain of length L, which is initially filled with oil ($S = 1$ for $0 < x < L$ at $t = 0$). Water is injected at the left boundary ($S = 0$ at $x/L = 0$ for $t > 0$) at a constant volume flow rate of ϕU. Figure 1(*a*) depicts the total and trapped oil saturation spatial profiles after the time $t = 0.5\tau_x$ for $\overline{\tau}_{z_o} = 10^{-2}\tau_x$. It can be observed that below $S \approx 0.3$ almost all the oil is immobile. Figure 1(*b*) shows the effective oil relative permeability ($k^e_{r_o} = (1 - \zeta/S)k_{r_o}$) curves for varying $\overline{\tau}_{z_o}$. In the limit of infinite trapping rate ($\overline{\tau}_{z_o} \to 0$), S_c approaches the residual saturation. Further, note that, as expected the saturations in figures 1(*a*) and 1(*b*) for $\overline{\tau}_{z_o} = 10^{-2}\tau_x$, below which oil is almost completely immobile, coincide.

More interesting cases are those with combined drainage and imbibition, where a hysteresis in the relative permeability can be observed. Therefore we consider a

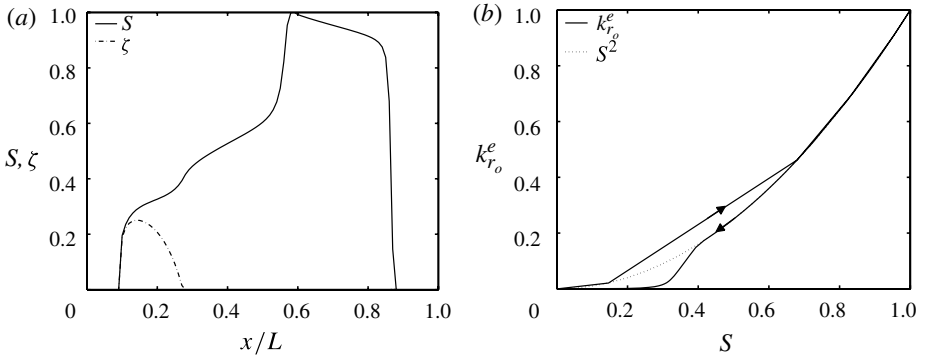

FIGURE 2. One-dimensional simulation results of the displacement of an oil plume by water after the time $t = 0.25\tau_x$ for $\overline{\tau}_{z_o} = 10^{-1}\tau_x$: (*a*) total oil saturation (S) and trapped oil saturation ζ; (*b*) effective relative permeability $k^e_{r_o} = (1 - \zeta/S)k_{r_o}$ curves for drainage (increasing S) and imbibition (decreasing S).

domain of length L, which initially (at $t = 0$) contains a plume of oil ($S = 1$) located between $x = 0.1L$ and $x = 0.6L$ and the rest of it is filled with water. At the left boundary, water is injected ($S = 0$ at $x = 0$ for $t > 0$) at a constant volume flow rate ϕU. Figure 2(*a*) depicts the total and trapped oil saturation profiles after the time $t = 0.25\tau_x$ for $\overline{\tau}_{z_o} = 10^{-1}\tau_x$. Note that trapping occurs only near the imbibition front (near the drainage the trapping is negligible), thereby being consistent with the physics of two-phase displacement in porous media. Next, in figure 2(*b*), the effective oil relative permeability as a function of oil saturation is plotted. During drainage (increasing S), the $k^e_{r_o}$-curve follows the equilibrium relative permeability ($k_r = S^2$), except across the shock, where it is connected by two points on the S^2-curve satisfying the Rankine–Hugoniot condition (LeVeque 1992). However, during imbibition (decreasing S) the $k^e_{r_o}$-curve follows the S^2-curve only till a point below which it bifurcates, following a different path. Note that the bifurcation and the trapping occur at the same saturation value.

6. Rapid ganglion mobilization and trapping ($\tau_v \gg \tau_n \ll \tau_x$)

If the rates of ganglion mobilization and trapping are much higher than the rates of convection, coalescence and breakup, only the equilibrium distribution of $N(t)$ is required to close the MDF-equation. Though in general this assumption does not lead to a closed set of moment transport equations, it is worth analysing such a case, especially from a numerical viewpoint. Taking the limits $\tau_n/\tau_x \to 0$ and $\tau_n/\tau_v \to 0$ in (3.10) gives

$$\mathscr{G}(\boldsymbol{x}, v, n, a; t) = \frac{\alpha_M \delta_{n1} + \alpha_T \delta_{n0}}{\alpha_M + \alpha_T} \mathscr{H}(\boldsymbol{x}, v, a; t) \tag{6.1}$$

for the JPDF of $\boldsymbol{X}(t)$, $V(t)$, $N(t)$ and $A(t)$, where $\mathscr{H}$ is the JPDF of $\boldsymbol{X}(t)$, $V(t)$ and $A(t)$. Since $N(t)$ varies much faster than $V(t)$, the parameters τ_v, σ^2 and V^{eq} can be assumed to be independent of n. By applying the operator $\sum_{n\in\mathbb{I}^1}$ to (3.10) and using (6.1) one obtains

$$\frac{\partial \mathscr{H}}{\partial t} + \frac{\partial}{\partial x_i}\left\{ -\left(\frac{\alpha_M}{\alpha_M + \alpha_T}\right) \frac{k_{r_a} k}{\phi S_a \mu_a} \left(\frac{\partial p}{\partial x_i} + \rho_a g e_{z_i}\right) \mathscr{H} \right\}$$

$$+\frac{\partial}{\partial v}\left\{-\frac{v}{\tau_v}\left(\log\frac{v}{V^{eq}}-\frac{\sigma^2}{2}\right)\mathscr{H}\right\}$$
$$=\frac{\partial^2}{\partial x_i^2}\{\Gamma|\boldsymbol{u}|\mathscr{H}\}+\frac{\partial^2}{\partial v^2}\left\{\frac{v^2\sigma^2}{\tau_v}\mathscr{H}\right\}, \tag{6.2}$$

which is a Fokker–Planck equation for $\mathscr{H}$. An important characteristic of (6.2) is that unlike (2.3) the particle velocity is described by a continuous stochastic process, i.e.

$$\boldsymbol{U}=-\frac{\alpha_M(V)}{\alpha_M(V)+\alpha_T(V)}\frac{k_{r_A}k}{\phi S_A\mu_A}(\nabla p_A+\rho_A g\boldsymbol{e}_z), \tag{6.3}$$

which can be considered as a time-averaged ganglion velocity (over the time scale τ_n). A number of experimental and pore-scale simulation-based studies show that for a given capillary number and viscosity ratio this velocity is a strong function of ganglion size (Hinkley, Dias & Payatakes 1987; Dias & Payatakes 1986*b*). Here it is modelled by (6.3), where the dependence on ganglion size is via the parameters α_M and α_T. Furthermore, it has been observed that for a given pressure gradient and saturation, the time-averaged ganglion velocity tends asymptotically to a constant value as the ganglion size increases. This is evident from (6.3) as α_T/α_M vanishes for very big ganglia.

Note that the model (6.2) resembles the non-equilibrium mobility model proposed by Tyagi *et al.* (2008). Here the particle mobility is a function of the ganglion size, which evolves according to a Langevin equation (2.10). In general, the moment equations derived from (6.2) do not lead to a closed set of equations and additional closure assumptions would be required. The model is advantageous for the numerical calculations, if the mobilization and trapping rates are very high; therefore, the time step size is not restricted due to the rule (2.6).

7. Simulation results

Here, some one- and two-dimensional numerical simulation results obtained with the full stochastic model as described in §§ 2 and 3, are presented. For all simulations, incompressible flow of two immiscible fluids (e.g. oil and water or CO_2 and brine) through a homogeneous isotropic porous medium (constant k and ϕ) is considered. The wetting phase (brine or water) is assumed to be connected throughout the porous medium and the non-wetting phase (oil or CO_2) can either be connected or disconnected (depending on the saturation). In this section, the non-wetting-phase saturation is denoted by S and the subscripts o and w indicate non-wetting and wetting phases, respectively. For simulations quadratic relative permeabilities were employed, i.e. $k_{r_o}=S^2$, $k_{r_w}=(1-S)^2$ (Spiteri *et al.* 2008), and the macroscopic capillary pressure was ignored. Note that more general relative permeability functions may be employed to better describe a particular flow scenario (Avraam & Payatakes 1995*b*; Blunt *et al.* 2002; Piri & Blunt 2005). However, here for the demonstration of the concept, we limit ourselves only to these simple power-law functions.

The stochastic models depend on several parameters, which could, for example, be obtained from pore-scale simulation studies or experiments. However, as mentioned before, the goal of this paper is to demonstrate the concept; therefore, only results for assumed parameters are presented. The test cases are designed to illustrate how the parameters, which characterize the pore-scale dynamics, influence the macro-scale dynamics, while the main focus is on the finite rate effects due to coalescence and breakup. Constant τ_v and σ^2 were used for all the simulations and the mean

equilibrium ganglion size is given by

$$V^{eq}(S) = \begin{cases} V^{eq}_{min}\left(\dfrac{V^{eq}_{max}}{V^{eq}_{min}}\right)^{S/S_c} & \text{if } 0 < S < S_c \\ V^{eq}_{max}\mathrm{e}^{5(S-S_c)} & \text{if } S_c \leqslant S \leqslant 1, \end{cases} \tag{7.1}$$

where V^{eq}_{min} and V^{eq}_{max} denote minimum and maximum mean equilibrium ganglion size, respectively, and S_c is the saturation below which the non-wetting phase is disconnected. Further, α_M and α_T are assumed to be power-law functions of ganglion size, i.e. $\alpha_M = C_m v^p$ and $\alpha_T = C_t v^q$, where C_m and C_t are two constants. These relations are in agreement (qualitatively) with the physics of ganglion motion according to which a smaller ganglion gets easily trapped and a bigger ganglion gets easily mobilized (for example, see Larson *et al.* 1977).

The stochastic particle method (SPM), which was proposed by Tyagi *et al.* (2008) and also briefly described in § 1, is employed to simulate the flow. The algorithm comprises solving the pressure equation (3.16) on a finite volume grid and transporting computational particles in the physical domain and various probability spaces according to the stochastic rules (2.5), (2.6) and (2.8). The particle velocities are written in fractional flow formulation to guarantee local average mass balance during a simulation (Tyagi *et al.* 2008; Tyagi & Jenny 2011). To avoid time stepping errors, the transition probabilities (2.6) are calculated as (Gillespie 1991):

$$\mathrm{Prob}(N : 0 \to 1; \Delta t) = 1 - \mathrm{e}^{-\alpha_M \Delta t} \quad \text{and} \quad \mathrm{Prob}(N : 1 \to 0; \Delta t) = 1 - \mathrm{e}^{-\alpha_T \Delta t}. \tag{7.2}$$

However, for a desired accuracy, still sufficiently small time steps are required. Since the focus of this paper is on showing the modelling potential of the PDF-approach, for numerical and computational details we refer to Tyagi *et al.* (2008), Jenny *et al.* (2001) and Rembold & Jenny (2006).

7.1. *One-dimensional simulations*

The following simulations were performed on a uniform one-dimensional grid with spacing $\mathrm{d}x = 0.01L$, and to ensure numerical stability, a time step $\mathrm{d}t = 5 \times 10^{-3}\tau_x$, which corresponds to a maximum CFL number of 0.5, was chosen. To obtain smooth stochastic moments, a huge number of particles was employed, i.e. an average of approximately 50 000 particles per cell. All simulations were performed with $\sigma^2 = 0.25$, $V_{min} = 0.05V_0$, $V_{max} = V_0$, $S_c = 0.4$, $p = -q = 1$ and $\mu_o/\mu_w = 1$.

First, we consider an imbibition displacement problem (e.g. water displacing oil), where a domain of length L is initially filled with oil ($S = 1$ for $0 < x < L$ at $t = 0$) and water is injected at the left boundary ($S = 0$ at $x = L$ for $t > 0$) at a constant volume flow rate of ϕU. Initially, all oil-phase particles are mobile and represent the same size V_0. The coefficients of mobilization and trapping rates are: $C_m = 40/(V_0\tau_x)$ and $C_t = 5V_0/\tau_x$. Figures 3(*a*) and 3(*b*) depict the total and trapped oil saturations for varying τ_v after the time $t = 0.5\tau_x$ and one can observe that both significantly increase as τ_v is increased. Note that for $\tau_v/\tau_x \to 0$, the rapid coalescence–breakup solution (§ 5) is recovered with the average mobilization and trapping rates

$$\beta_M = C_m V^{eq} \quad \text{and} \quad \beta_T = (C_t/V^{eq})\mathrm{e}^{\sigma^2}. \tag{7.3}$$

Figures 4(*a*) and 4(*b*) show spatial profiles of mean and variance of ganglion size (both normalized with their equilibrium values) for varying τ_v after the time $t = 0.5\tau_x$. While for a smaller τ_v/τ_x both mean and variance remain close to their equilibrium

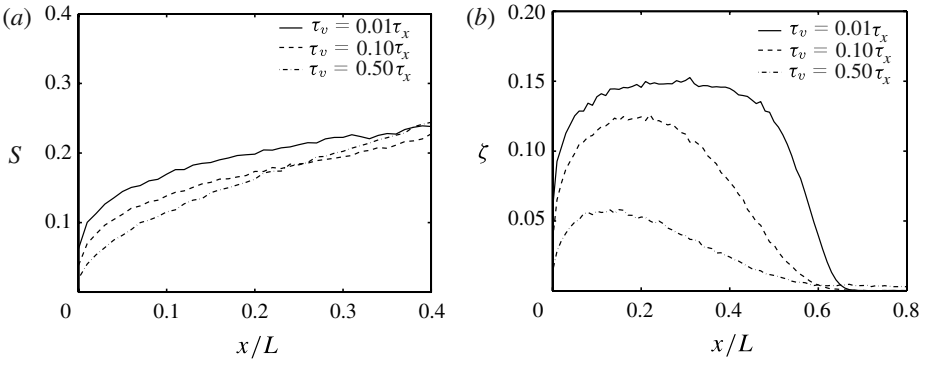

FIGURE 3. One-dimensional imbibition simulation results for varying τ_v after the time $t = 0.5\tau_x$: (*a*) overall oil saturation (S); (*b*) trapped oil saturation ζ.

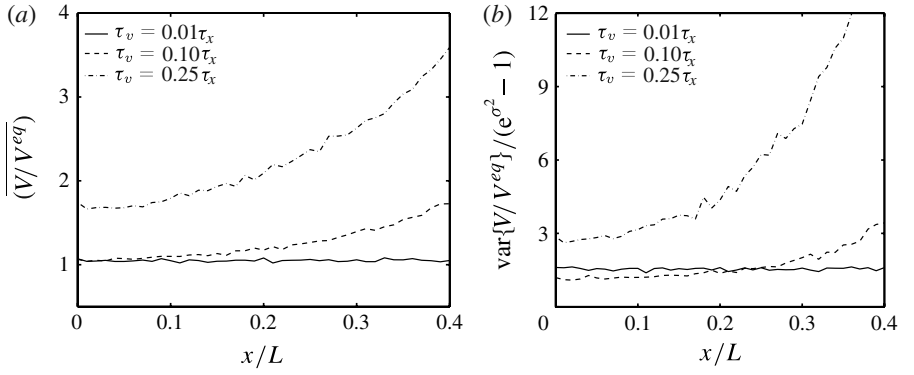

FIGURE 4. One-dimensional imbibition simulation results for varying τ_v after the time $t = 0.5\tau_x$: (*a*) normalized mean ganglion size; (*b*) normalized variance of the ganglion size.

values, for $\tau_v \geqslant \tau_x$ a significant deviation can be observed. Further, this deviation increases in the downstream direction. A similar trend can be observed for the marginal PDFs of $V(t)$, which are depicted in figures 5(*a*) and 5(*b*) after the time $t = 0.5\tau_x$ at the locations $x = 0.2L$ and $x = 0.4L$, respectively. The departure from equilibrium is solely due to finite-rate coalescence–breakup kinetics. Recall that τ_v is the characteristic time scale of the process $V(t)$ to reach the equilibrium distribution (which is here a function of saturation). Consequently, for $\tau_v \ll \tau_x$ the PDF of V remains close to equilibrium, but this is not the case if $\tau_v \geqslant \tau_x$.

Next, buoyancy-driven flow in which both drainage and imbibition occur is considered. This scenario can be regarded as the idealization of the post-injection phase of CO_2 storage in a brine aquifer. The initial configuration and geometrical details are shown in figure 6, where no-flow boundary conditions are applied at $z = 0$ and $z = H$. The CO_2 phase, being lighter than the brine, migrates upwards leading to drainage near the leading front and imbibition in the trailing region. To simulate this case, uniformly distributed particles of equal mass are launched in the domain such that at $t = 0$: $S = 1$ and $A = o$ (CO_2 phase), if $0.1H \leqslant z \leqslant 0.3H$, and $S = 0$ and $A = w$ (brine phase) else. Figures 7(*a*) and 7(*b*) depict profiles of total and trapped CO_2 saturations at two different times for $\tau_v = 0.25\tau_x$, $C_m = 40/(V_0\tau_x)$ and $C_t = 5V_0/\tau_x$.

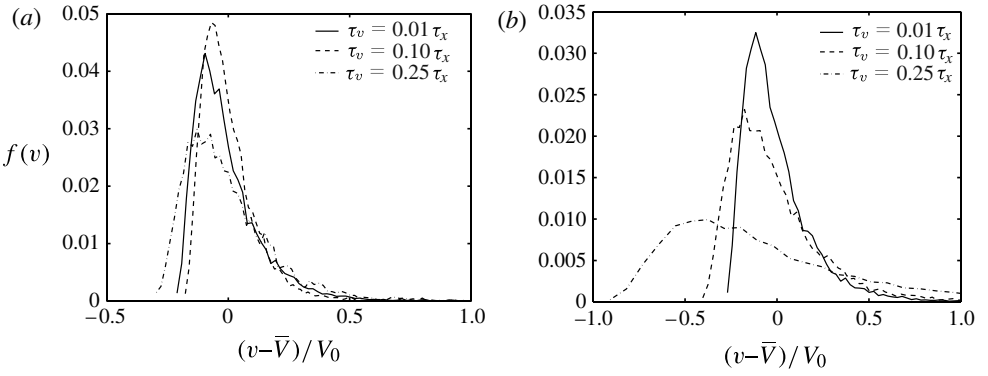

FIGURE 5. Marginal PDFs of the ganglion size for varying τ_v after the time $t = 0.5\tau_x$ and at the location: (*a*) $x = 0.2L$; (*b*) $x = 0.4L$.

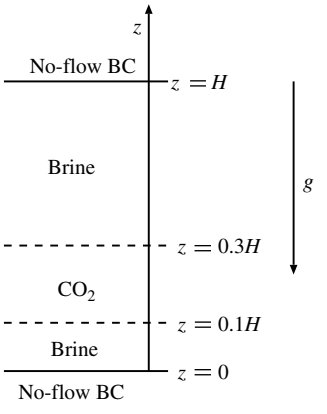

FIGURE 6. Geometry and initial distribution of the phases in the one-dimensional model for buoyancy-driven flow.

Although trapping also takes place at the drainage front, it is much more pronounced in the trailing region, especially at the later times. The underlying dynamics can be better explained with the ganglion size distributions. The mean and variance of V are shown in figures 8(*a*) and 8(*b*), while the distributions of the trapped and mobile particles are depicted in figures 9 and 10, where the particle size is proportional to the ganglion size. For the sake of clarity, only a random subset of all particles is depicted. For a brief period, some of the CO_2 phase near the drainage front forms smaller ganglia (due to breakup), which get trapped. However, soon they grow in size (due to coalescence) and become mobile again. In the trailing region, where breakup dominates due to low CO_2 saturation, ganglia remain sufficiently small and hence almost all the CO_2 gets trapped.

Finally, results are presented to demonstrate the validity of the Fokker–Planck model in the limit of rapid ganglion mobilization and trapping (§ 6). Figure 11 depicts profiles of the mean CO_2 particle mobility for $\tau_v = 0.25\tau_x$, $C_m/C_t = 8/V_0^2$ and for varying $\tau_n = 1/(C_m V_0 + C_t/V_0)$ after the time $t = 4\tau_x$. Here, $\tau_n = 0$ corresponds to the Fokker–Planck model, in which particles evolve with the velocities given by (6.3). As expected, in the limit $\tau_n \to 0$, the mean mobility obtained with the full stochastic

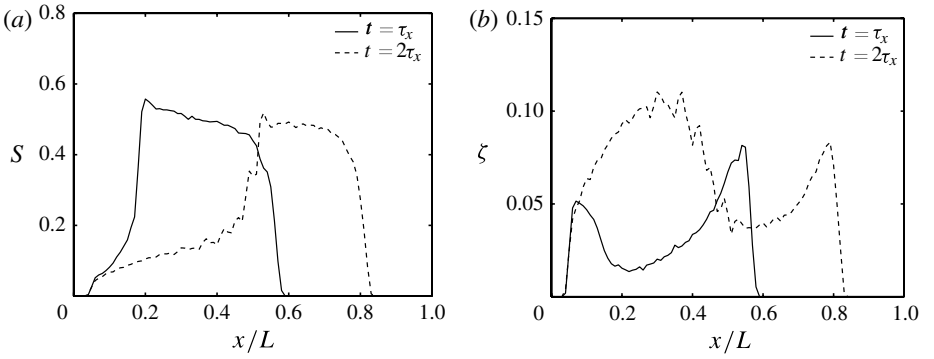

FIGURE 7. One-dimensional simulation results from the buoyancy-driven test case with $\tau_v = 0.25\tau_x$, $C_m = 40/(V_0\tau_x)$ and $C_t = 5V_0/\tau_x$: (*a*) total CO_2 saturation (S); (*b*) trapped CO_2 saturation ζ.

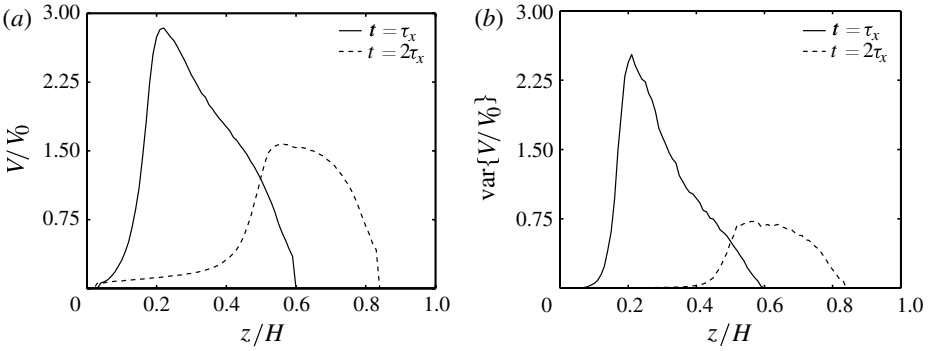

FIGURE 8. One-dimensional simulation results from the buoyancy-driven test case with $\tau_v = 0.25\tau_x$, $C_m = 40/(V_0\tau_x)$ and $C_t = 5V_0/\tau_x$: (*a*) mean CO_2 ganglion size; (*b*) variance of the CO_2 ganglion size distribution.

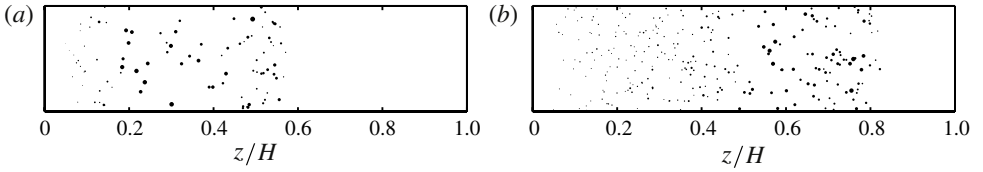

FIGURE 9. Trapped CO_2 particle distribution in the one-dimensional simulation of buoyancy-driven flow with $\tau_v = 0.25\tau_x$, $C_m = 40/(V_0\tau_x)$ and $C_t = 5V_0/\tau_x$ after the time: (*a*) $t = \tau_x$; (*b*) $t = 2\tau_x$. Note that all particles actually lie on the z-axis. Only a fraction of all particles (one out of fifty) is shown.

model, where particles evolve with the velocities given by (2.3), converges to the Fokker–Planck (FP) solution.

7.2. *Two-dimensional simulations*

Although the basic physics of ganglion dynamics in two or three dimensions is similar to that in one dimension, it is worthwhile presenting studies of a two-dimensional

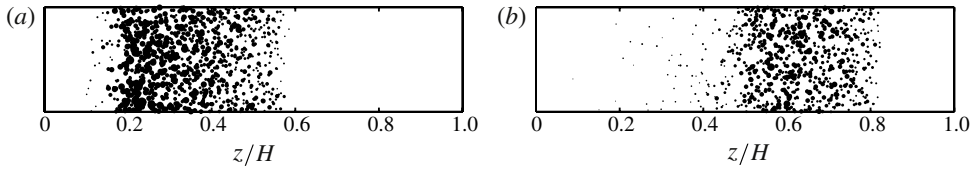

FIGURE 10. Mobile CO_2 particle distribution in the one-dimensional simulation of buoyancy-driven flow with $\tau_v = 0.25\tau_x$, $C_m = 40/(V_0\tau_x)$ and $C_t = 5V_0/\tau_x$ after the time: (*a*) $t = \tau_x$; (*b*) $t = 2\tau_x$. Note that all particles actually lie on the z-axis. Only a fraction of all particles (one out of fifty) is shown.

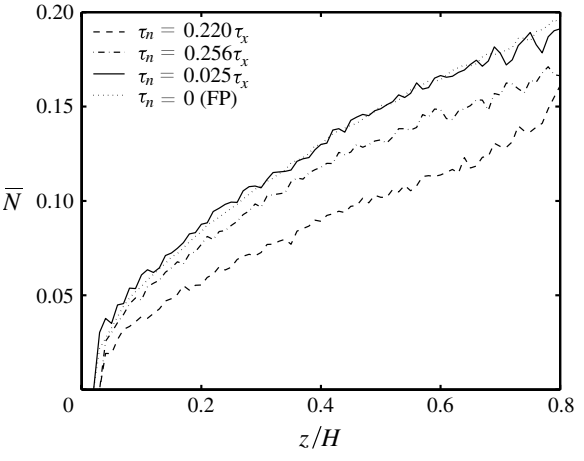

FIGURE 11. Mean CO_2 mobility spatial profiles in the one-dimensional simulation of buoyancy-driven flow with varying $\tau_n = 1/(C_m V_0 + C_t/V_0)$ after the time $t = 4\tau_x$. Here $\tau_n = 0$ corresponds to the Fokker–Planck (FP) solution (6.2).

test case. For this purpose the rectangular domain shown in figure 12 is considered. It has a width of L and a height of $H = L$. Initially (at $t = 0$), the centre of a circular CO_2 plume ($S = 1$) with radius $r = 0.2L$ was located $0.25H$ below the centre of the domain. At $t = 0$ the particles were uniformly distributed in the domain and their phase indicators were set to o inside the circle and w otherwise. At all boundaries no-flow conditions were applied and a uniform orthogonal grid consisting of 100×100 cells was employed to solve the pressure equation and to sample and represent stochastic moments. The time step was chosen such that the CFL condition is satisfied everywhere. In order to obtain smooth stochastic moments, an average of 4000 particles per cell were employed. The simulations were performed with $C_m = 40/(V_0\tau_x)$, $C_t = 5V_0/\tau_x$, $\sigma^2 = 0.25$, $V_{min} = 0.05V_0$, $V_{max} = V_0$, $S_c = 0.4$, $p = -q = 1$ and $\mu_o/\mu_w = 1$.

First, results are presented for $\tau_v = 0.25\tau_x$ to show the effect of trapping on the general multi-phase flow dynamics. Figure 13 depicts the time evolution of CO_2 particles with and without trapping, where for the sake of clarity only a random subset of all particles is depicted. In both cases, as the plume migrates upwards, a trail of CO_2 is left behind; this represents the imbibition expansion fan. Upon reaching the ceiling, the CO_2 particles start to move laterally. It can be observed that trapping leads to a high concentration of CO_2 particles in the trail. Figures 14(*a*) and 14(*b*) depict

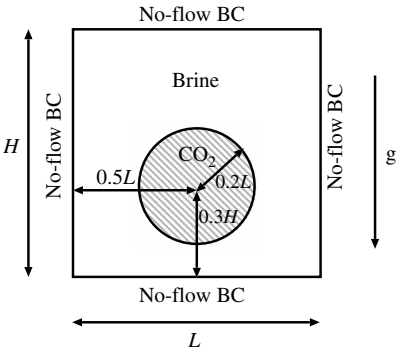

FIGURE 12. Geometry and initial distribution of the phases in the two-dimensional model of buoyancy-driven flow.

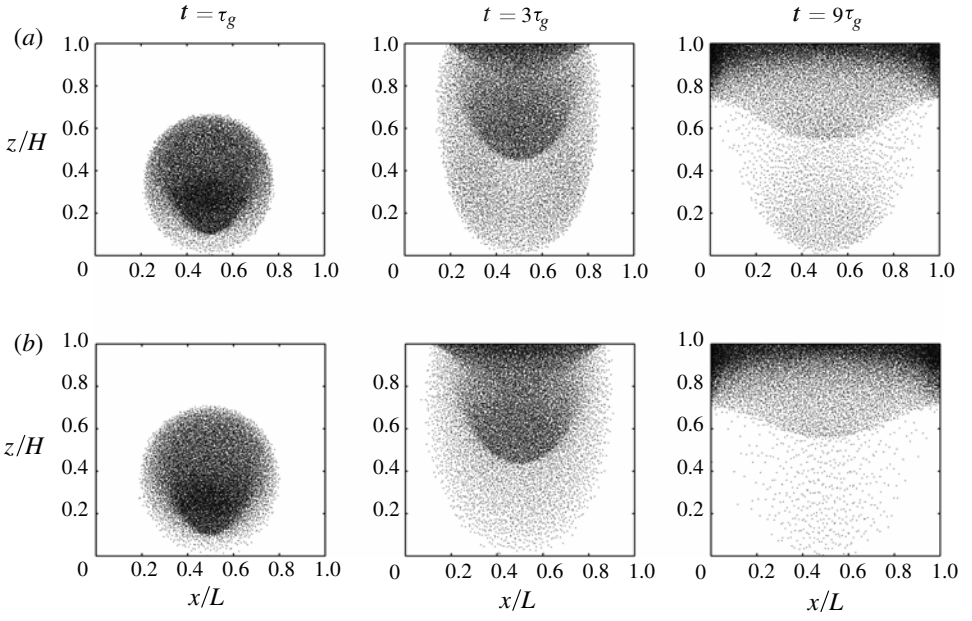

FIGURE 13. Time evolution of CO_2 particle spatial distribution: (*a*) with trapping; (*b*) without trapping. Only a fraction of all particles (one out of fifty) is shown.

the trapped and mobile CO_2 particle distributions in the imbibition trail after the time $t = 8\tau_x$; the size of the particles represents the corresponding ganglion size. Notice that in general trapped ganglia are smaller in size than mobile ganglia.

Next, similar to the one-dimensional case, some results are presented to show the influence of τ_v on CO_2 trapping. Figures 15(*a*) and 15(*b*) depict the trapped CO_2 saturation for $\tau_v = 0.01\tau_x$ and $\tau_v = 0.25\tau_x$, respectively, after the time $t = 2\tau_x$. The saturation of trapped CO_2 is significantly higher in the near-equilibrium case than in the non-equilibrium case, which is consistent with the corresponding maps of the normalized mean ganglion size shown in figures 16(*a*) and 16(*b*).

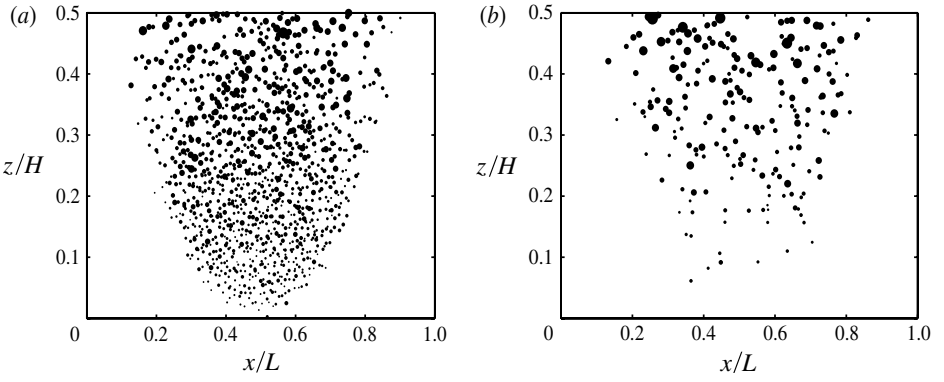

FIGURE 14. CO_2 particle spatial and size distribution after the time $t = 8\tau_x$: (*a*) trapped particles; (*b*) mobile particles. Only a fraction of all particles (one out of fifty) is shown.

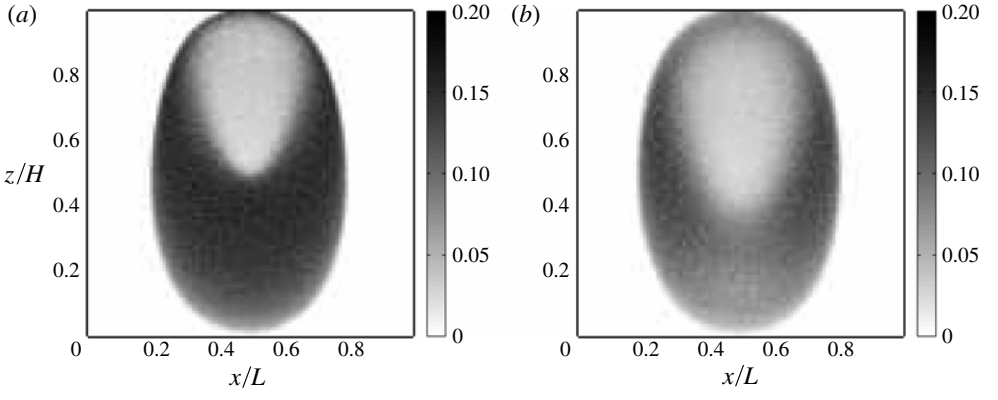

FIGURE 15. Trapped CO_2 saturation after the time $t = 2\tau_x$: (*a*) $\tau_v = 0.01\tau_x$; (*b*) $\tau_v = 0.25\tau_x$.

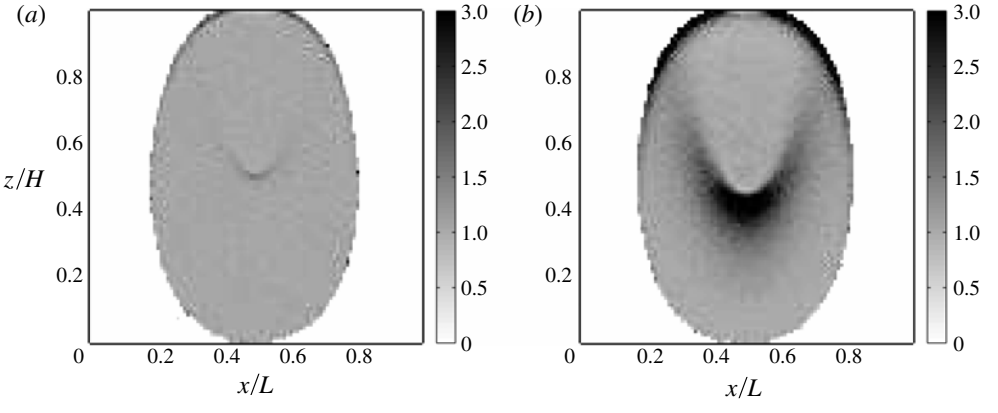

FIGURE 16. Normalized mean CO_2 ganglion size after the time $t = 2\tau_x$: (*a*) $\tau_v = 0.01\tau_x$; (*b*) $\tau_v = 0.25\tau_x$.

8. Discussion

We adopted a PDF-approach to model the motion of ganglia in multi-phase flow through porous media, where ganglia undergo events such as mobilization, trapping, coalescence and breakup. The resulting pore-scale ganglion dynamics is modelled with a set of Markov stochastic processes, which are characterized by equilibrium distributions and correlation times. Several analytical and numerical examples are presented to demonstrate the important fact that the nonlinearity, PDFs and correlation times in the microscopic flow can have a significant influence on the macroscopic flow, which is often ignored in traditional constitutive models. It has to be emphasized, however, that these examples only serve to demonstrate the concept, generality, advantages and capabilities of the PDF-approach in modelling complex non-equilibrium phenomena; at this point the model lacks a proper calibration. Nevertheless, in the current work a consistent framework is presented, which together with pore-scale simulation studies and/or measurements can lead to the development of better macroscopic models. A brief discussion of the modelling issues that may require further investigation and improvement follows.

8.1. *Ganglion mobility*

The present model for ganglion mobility assumes that a ganglion either is trapped or moves with the Darcy velocity. However, the latter is a very strong assumption and in fact, it has been observed that the ganglion velocity is different from that in the connected phase (for the same pressure gradient and saturation). To account for this difference, one might assume that the mobile ganglion mobility, $\tilde{\Lambda}$, drifts towards the Darcy mobility at a rate $1/\tau_\lambda$, i.e.

$$\mathrm{d}\tilde{\Lambda} = \frac{(\tilde{\Lambda} - k_{r_A}/S_A)}{\tau_\lambda}\,\mathrm{d}t. \tag{8.1}$$

The particle mobility is then defined as

$$\Lambda = N\tilde{\Lambda}. \tag{8.2}$$

Note that the model (2.4) is recovered in the limit of $\tau_\lambda \to 0$.

8.2. *Statistics extraction*

In appendix A, the strategy to use micro-scale information from the birth–death model for computing the parameters, such as mobilization and trapping rates and equilibrium PDF, in the PDF-approach is demonstrated. However, one could also determine these quantities from pore-scale simulations or from experiments; a possible strategy for this would involve the following steps.

(*a*) For example, if log-normal equilibrium distributions of V are assumed, only means and variances have to be determined. One possibility would be to employ pore-scale simulations, where a statistically one-dimensional column is considered with constant pressure values at inlets and outlets, and prescribed saturation at the inlet. The column has to be long enough that equilibrium ganglion size distribution is reached at the outlet.

(*b*) If the distribution is not in equilibrium at the inlet, the time scale for the PDF relaxation can be extracted.

(*c*) During the whole simulation one can extract conditional trapping rates.

(*d*) During the whole simulation one can extract conditional mobilization rates.

With this extracted information the PDF-approach would not only reproduce the pore-scale simulation results (up to the level of modelled statistics), but allow one to perform large-scale simulations, which is not possible with a pore-scale simulator (computational cost). Therefore, the PDF-approach acts as a mediator between pore and Darcy scales.

9. Conclusion

The present PDF-approach is a general framework, which allows one to build macroscopic models based on microscopic (ganglion) dynamics for non-equilibrium flows, and furthermore, it provides a convenient computational method (i.e. SPM) for simulation. Moreover, since the PDF-approach is based on sound mathematical grounds, it is a consistent framework to translate physical observations or phenomena into mathematical models while clearly stating the assumptions and approximations made. The PDF-approach requires the Lagrangian evolution of stochastic variables in a probability space which is chosen according to the problem requirements. Such evolutions can be constructed based on the known Lagrangian statistics of ganglia flow, e.g. from pore-scale simulations/experiments or birth–death type population balance models. It was shown how mobilization and trapping rates can be derived from a birth–death type formalism. Also, the assumption of approximating the discontinuous ganglion size process, due to successive ganglia coalescence and breakup, by a continuous process is verified for the case of steady-state fully developed flow.

One of the main objectives of this paper was to demonstrate the importance of fluctuations and correlations in modelling nonlinear porous media flows. Indeed the closure problem that arises with an Eulerian deterministic macroscopic modelling approach is a natural consequence of the nonlinear microscopic flow physics. Such nonlinear effects are present in the ganglia flow; both mobilization–trapping and coalescence–breakup are nonlinear phenomena at the pore scale.

The PDF-approach also allows us to investigate the flow behaviour in special cases, e.g. for very short correlation times. In a scenario with several coupled stochastic processes, if one process is much faster than the others, only the equilibrium distribution of the faster process is sufficient to describe the flow, thereby reducing the dimensionality of the governing MDF-equation. For quasi-uniform flows, the saturation transport equation appears in closed form with the mean mobility fully determined, if the equilibrium PDFs are known. A two-equation transport model (one equation for the saturation and one for the mean mobility) is obtained in the limit of very fast coalescence and breakup processes. Interestingly, this model is very similar to the non-equilibrium models given by other researchers. However, we have derived this in a rigorous way by clearly showing the necessary assumptions and approximations. Furthermore, using this model, the well-known phenomenon of relative permeability hysteresis, which arises due to finite-rate mobilization and trapping, can easily be explained. Finally, with the help of some one- and two-dimensional simulation results, we have shown the importance of correlation times and distributions on the large-scale flow behaviour.

Appendix A. Comparison with birth–death population balance equations

The discontinuous Markovian ganglion size process (due to breakup and coalescence), which is modelled with the birth–death approach (Payatakes *et al.* 1980), is replaced by a continuous Markovian process in the PDF-approach (§ 2.4). Here the validity of this replacement is examined. Moreover, the following analysis provides

expressions for mobilization and trapping rates in terms of the quantities which appear in the birth–death population balance equations. The mathematical developments of birth–death formulations are presented only briefly; more detailed explanations can be found in the paper by Valavanides *et al.* (1998). Without loss of generality it is assumed that flow is spatially uniform; consequently, all spatial dependences can be ignored.

Let $f_0^{nd}(v;t)\,\mathrm{d}v$ and $f_1^{nd}(v;t)\,\mathrm{d}v$ be the numbers per unit reservoir volume of trapped and mobile ganglia, which have a volume between v and $v+\mathrm{d}v$, respectively. The number densities $f_{0,1}^{nd}(v;t)$ are related to the conditional ganglion size PDFs as

$$f_0^{nd}(v;t) = q_0 f(v \mid n=0;t) \quad \text{and} \quad f_1^{nd}(v;t) = q_1 f(v \mid n=1;t), \tag{A 1}$$

where q_0 and q_1 are the numbers (per unit reservoir volume) of mobile and trapped ganglia, respectively. According to the birth–death model by Payatakes *et al.* (1980), a trapped ganglion can become mobile only through coalescence with a mobile ganglion. Thus, the number of ganglia mobilizing during the time $\mathrm{d}t$ whose volumes are between v and $v+\mathrm{d}v$ is given by $\alpha_M(v;t)f_0^{nd}(v;t)\,\mathrm{d}v\,\mathrm{d}t$, where

$$\alpha_M(v;t) = S_o co \int_0^\infty R^{01}(v,w) f_1^{nd}(w;t)\{1-s(v+w)\}\,\mathrm{d}w \tag{A 2}$$

is the mobilization rate. Here S_o is the non-wetting-phase saturation, co the coalescence factor, $R^{01}(v,w)$ the collision kernel and $s(v)$ the trapping probability of a newly formed v-ganglion. Note that the newly formed $(v+w)$ ganglion becomes mobile with probability $1-s(v+w)$. A mobile ganglion can get trapped in three ways: by stranding; by breaking up into two daughter ganglia, where both or one of the daughter ganglia may strand; and by coalescing with an already trapped ganglion, where the resulting ganglion may strand. There is also a fourth possibility, in which two mobile ganglia coalesce and the resulting ganglion may strand; however, this case was ignored by Payatakes *et al.* (1980) and the same is done here. Thus, during the time $\mathrm{d}t$, the number of ganglia getting trapped, whose volumes are between v and $v+\mathrm{d}v$, is given by $\alpha_T(v;t)f_1^{nd}(v;t)\,\mathrm{d}v\,\mathrm{d}t$, where

$$\alpha_T(v;t) = \lambda(v)u + \frac{\phi(v)u}{2}\int_0^v W(v,w)\left\{\frac{ws(w)+(v-w)s(v-w)}{v}\right\}\mathrm{d}w + S_o co\int_0^\infty R^{10}(v,w)s(v+w)f_0^{nd}(w;t)\,\mathrm{d}w \tag{A 3}$$

is the trapping rate. Here λ is the stranding rate, u the ganglion velocity, ϕ the breakup rate, $W(v,w)$ the breakup mode probability and due to symmetry, $R^{10}(v,w) = R^{01}(v,w)$. The expressions (A 2) and (A 3) indeed show how the two macroscopic parameters α_M and α_T in the PDF-approach can be derived from a micro-scale description.

The two population balance equations (Valavanides *et al.* 1998) can also be written as

$$\frac{\partial f_0^{nd}(v;t)}{\partial t} = \alpha_T(v;t)f_1^{nd}(v;t) - \alpha_M(v;t)f_0^{nd}(v;t) + \mathscr{E}_0(v;t) \tag{A 4}$$

and

$$\frac{\partial f_1^{nd}(v;t)}{\partial t} = \alpha_M(v;t)f_0^{nd}(v;t) - \alpha_T(v;t)f_1^{nd}(v;t) + \mathscr{E}_1(v;t), \tag{A 5}$$

for trapped and mobile ganglia subpopulations, respectively. Here $\mathscr{E}_0(v;t)$ and $\mathscr{E}_1(v;t)$ account for the effect on ganglion size other than trapping and mobilization. Since the total volume of each subpopulation can only change due to mobilization or trapping, the relations

$$\int_0^\infty v\mathscr{E}_0(v;t)\,\mathrm{d}v = \int_0^\infty v\mathscr{E}_1(v;t)\,\mathrm{d}v = 0 \tag{A 6}$$

must hold at all times. Moreover, the volume of all ganglia must remain constant, i.e.

$$\int_0^\infty v f_0^{nd}(v;t)\,\mathrm{d}v + \int_0^\infty v f_1^{nd}(v;t)\,\mathrm{d}v = \text{constant}. \tag{A 7}$$

If ρ_o is the density of oil, which is assumed to be a constant here, by multiplying (A 4) and (A 5) with $\rho_o v$, the evolution equations for the mass density function $\mathscr{F}(v,n;t)$ for the trapped and mobile ganglia subpopulations are obtained:

$$\frac{\partial\mathscr{F}(v,0;t)}{\partial t} = \alpha_T(v;t)\mathscr{F}(v,1;t) - \alpha_M(v;t)\mathscr{F}(v,0;t) + \rho_o v\mathscr{E}_0(v;t) \tag{A 8}$$

and

$$\frac{\partial\mathscr{F}(v,1;t)}{\partial t} = \alpha_M(v;t)\mathscr{F}(v,0;t) - \alpha_T(v;t)\mathscr{F}(v,1;t) + \rho_o v\mathscr{E}_1(v;t), \tag{A 9}$$

respectively. In the PDF-approach, the last term in each of the above two equations is modelled by a Fokker–Planck-equation-type drift and diffusion in v-space, i.e. the approximations

$$\begin{aligned} v\mathscr{E}_0(v;t) = &-\frac{\partial}{\partial v}\{(D^v \mid n=0)\mathscr{F}(v,n=0;t)\} \\ &+ \frac{\partial^2}{\partial v\partial v}\{D^{v,v} \mid n=0\mathscr{F}(v,n=0;t)\} \end{aligned} \tag{A 10}$$

and

$$\begin{aligned} v\mathscr{E}_1(v;t) = &-\frac{\partial}{\partial v}\{(D^v \mid n=1)\mathscr{F}(v,n=1;t)\} \\ &+ \frac{\partial^2}{\partial v\partial v}\{D^{v,v} \mid n=1\mathscr{F}(v,n=1;t)\} \end{aligned} \tag{A 11}$$

are made. This indeed amounts to approximating a discontinuous Markovian process by a Markovian continuous process, which can always be modelled by a Fokker–Planck equation.

To demonstrate the basic modelling strategy followed in the PDF-approach, it is assumed that D^v and $D^{v,v}$ are independent of n, i.e. the ganglion size evolves independently of mobilization and trapping. With this assumption the summation of (A 8) and (A 9) yields

$$\frac{\partial\mathscr{F}(v,t)}{\partial t} = -\frac{\partial}{\partial v}\{D^v\mathscr{F}(v;t)\} + \frac{\partial^2}{\partial v\partial v}\{D^{v,v}\mathscr{F}(v;t)\}, \tag{A 12}$$

which is a Fokker–Planck equation for the marginal MDF $\mathscr{F}(v;t)$. This equation can be solved for $\mathscr{F}(v;t)$, if the coefficients D^v and $D^{v,v}$ are known, which indeed determine the stochastic process $V(t)$. The process $V(t)$ is constructed in a way such that the marginal MDFs obtained from the PDF- and the birth–death-approach are the

same. Here a statistically one-dimensional flow of ganglia, equivalent to steady-state fully developed (SSFD) flow (Valavanides *et al.* 1998), is considered. The birth–death population balance equations are solved until stationary state is obtained; an explicit first-order Runge–Kutta time integration scheme is employed for this purpose. The various parameters in the population balance equations are chosen as

$$\left.\begin{aligned} \lambda(v) &= \frac{1}{2}\exp(-v/2), \quad \phi(v) = v/2, \quad W(w,v) = \frac{2}{w}, \\ s(v) &= \frac{1}{2}\exp(-v/2), \quad u_z(v) = 1 \end{aligned}\right\} \tag{A 13}$$

and

$$R^{ij}(w,v) = \begin{cases} w+v & \text{if } i,j>0 \\ 0 & \text{if } i=j=0. \end{cases} \tag{A 14}$$

They qualitatively agree with those presented by Valavanides *et al.* (1998); however, note that their specific choice is not relevant here. From numerical studies with the birth–death model for a wide parameter range, it was found that the ganglion size PDFs (conditional and marginal) can be well approximated by a Gamma-PDF Therefore, the stochastic process

$$\mathrm{d}V(t) = -\frac{(V(t)-\langle V\rangle)}{\tau_v}\,\mathrm{d}t + \sqrt{\frac{2\sigma^2\langle V\rangle V(t)}{\tau_v}}\,\mathrm{d}W(t), \tag{A 15}$$

with constant σ and τ (which leads to a Gamma-PDF in equilibrium) is employed to model ganglion size (Pope 2003). In equilibrium, σ^2 is the variance of $V/\langle V\rangle$, $\langle V\rangle$ the mean and τ_v the autocorrelation time. From the birth–death solution, the mobilization and trapping rates, which are given by (A 2) and (A 3), respectively, are obtained as functions of v for a given value of co and S_o. These are plotted against ganglion size for three different oil saturation S_o values and for a coalescence factor of $co = 1$ (figures 17*a* and 17*b*). In this particular case, α_M significantly varies and α_T hardly changes, as S_o is altered. In addition to the rates α_M and α_T, the mean and variance of the ganglion size are required to close the model (A 15); these are shown in figure 18, where they are plotted against oil saturation. Both mean and variance increase as oil saturation increases. In figure 19(*a*), the marginal steady-state PDFs obtained from birth–death and PDF-approaches are shown for $co = 1$ and $S_o = 0.4$; they are in good agreement. Figure 19(*b*) compares the trapped ganglion volume fractions obtained from the two approaches as functions oil saturation; again a good agreement can be observed.

Appendix B. Small-$\overline{\tau}_\zeta$ approximation

The two-equation model, i.e. (5.17) and (5.18), is valid for any value of the relaxation time $\overline{\tau}_\zeta$; the standard equilibrium model is recovered for $\overline{\tau}_\zeta \to 0$ and the far from equilibrium situation for $\overline{\tau}_\zeta \to \infty$. However, many real-world non-equilibrium flow scenarios possess fast but finite time relaxation effects, i.e. $\overline{\tau}_\zeta/\tau_g < 1$. This fact can be exploited to explain some observed phenomena, which have been investigated by other approaches. To this end, we write $\overline{\tau}_\zeta(S) = \overline{\tau}'_\zeta(S)\tau_g\epsilon$, where $\overline{\tau}'_\zeta(S)$ is of order one and $\epsilon < 1$. ζ can be expanded as a formal series in powers of ϵ:

$$\zeta = \zeta_0 + \zeta_1\epsilon + \zeta_2\epsilon^2 + \cdots. \tag{B 1}$$

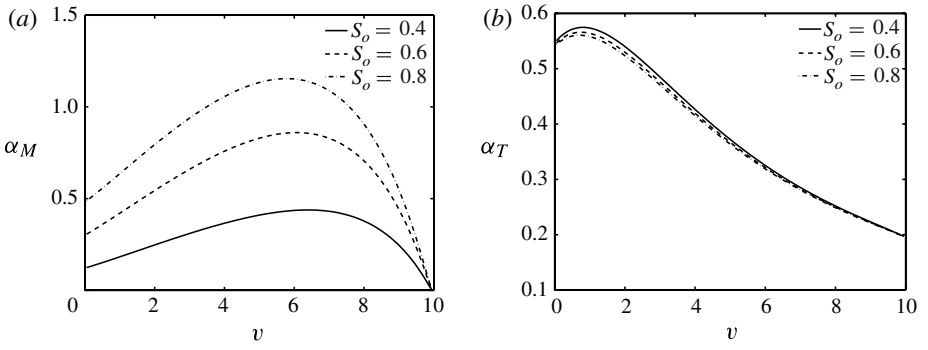

FIGURE 17. Stationary: (*a*) mobilization rate; (*b*) trapping rate, defined by (A 2) and (A 3), versus ganglion size for three different values of the oil saturation and for $co = 1$.

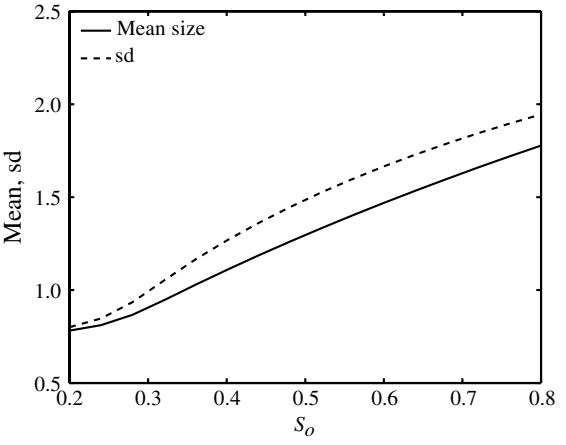

FIGURE 18. Mean and standard deviation (sd) of the ganglion size versus oil saturation for $co = 1$ as obtained from the birth–death model.

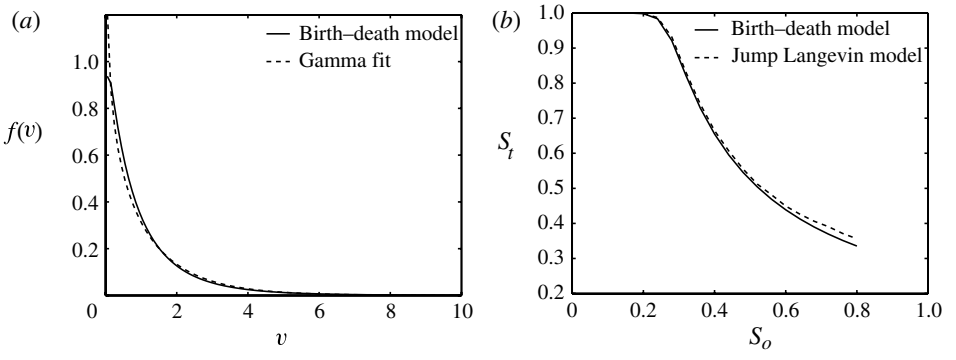

FIGURE 19. Comparison between the simulation results from the birth–death model and the PDF-approach (jump-Langevin model) in stationary state for $co = 1$: (*a*) marginal ganglion size PDF for $S_o = 0.4$; (*b*) trapped ganglia volume fraction (S_t) plotted against S_o.

Substituting this into (5.18) and subsequently equating the coefficients of each power of ϵ to zero gives

$$\zeta_0 = \zeta^{eq}, \quad \zeta_1 = -\tau_g \overline{\tau}'_\zeta(S)\frac{\partial \zeta^{eq}}{\partial t}, \quad \zeta_2 = -\tau_g \overline{\tau}'_\zeta(S)\frac{\partial \zeta_1}{\partial t}, \quad \cdots. \tag{B 2}$$

Substituting this back into (B 1) gives the following expression for ζ:

$$\zeta = \zeta^{eq} - \overline{\tau}_\zeta \frac{\partial \zeta^{eq}}{\partial t} + O(\epsilon^2), \tag{B 3}$$

which is truncated up to first-order in ϵ; the second- and higher-order terms will be ignored for the present analysis. Since ζ^{eq} is a known function of S (through mean mobilization and trapping rates), (B 3) can also be written as

$$\zeta = \zeta^{eq} - \overline{\tau}_\zeta \frac{\partial \zeta^{eq}}{\partial S}\frac{\partial S}{\partial t}, \tag{B 4}$$

in which the second term on the right-hand side accounts for dynamic effects. It has to be emphasized here that dynamic effects in the present model are due to non-equilibrium trapping and mobilization processes. There also exist very similar models, which account for dynamic effects in macroscopic capillary pressure (Hassanizadeh *et al.* 2002); however, they do not necessarily consider drainage–imbibition hysteresis effects due to trapping and mobilization. The relaxation time in the present model is related to the mobilization and trapping rates, which depend on the flow velocity, and hence on the flow time scale τ_g. Consequently, in some sense $\overline{\tau}_\zeta/\tau_g$ never vanishes. Thus, such a flow scenario, with dynamic mobilization and trapping will always be in non-equilibrium, irrespective of the magnitude of flow velocity (capillary number). Equation (B 4) shows how non-equilibrium trapping leads to hysteresis; the effective relative permeability depends on the flow direction. It is interesting to note that (B 4) is similar to many other relaxation models, e.g. the ones proposed by Barenblatt *et al.* (2003), Silin & Patzek (2004) and Schembre & Kovscek (2006), to describe non-equilibrium effects in relative permeability and macroscopic capillary pressure. However, here the macroscopic model parameters are rigorously derived from the microscopic physics by adopting a general statistical approach.

Recently, some effort has been made to model immiscible two-phase flow by separating the fluid into percolating and non-percolating parts, most notably the works of Hilfer (2006*b*,*a*) and Kats & Dujin (2001). In these approaches, the mass transfer rate between two parts of a phase is assumed to be proportional to time rate of saturation; however, this assumption is entirely phenomenological and has not been derived from the micro-scale physics. It can easily be shown that this assumption is a natural consequence of non-equilibrium trapping and mobilization. Using (5.18) and (B 4) for small $\overline{\tau}_\zeta$ (compared to τ_g), we can write

$$\frac{\partial \zeta}{\partial t} = \frac{\partial \zeta^{eq}}{\partial S}\frac{\partial S}{\partial t}, \tag{B 5}$$

which shows that the time rate of trapped oil saturation is proportional to the time rate of total oil saturation. In the present model, the mass transfer rate between the mobile and immobile parts of a phase is proportional to $(\zeta - \zeta^{eq})/\overline{\tau}_\zeta$.

The well-known relative permeability hysteresis, which is caused by non-equilibrium trapping and mobilization, comes out naturally from (B 4), if the effective relative permeability of oil ($k^e_{r_o} = (1 - \zeta/S)S^2$) is plotted against the water saturation $1 - S$. Let S_{oim} be the residual oil saturation and S_{wdr} the irreducible water saturation. It is natural

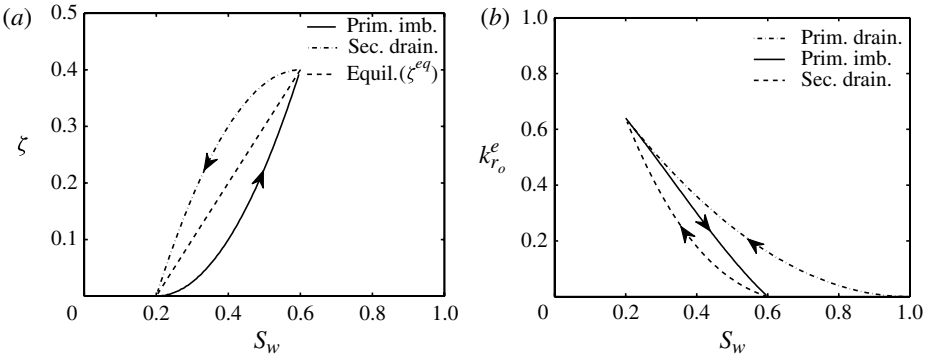

FIGURE 20. Relative permeability hysteresis as obtained from (B 4) during flow reversal: (*a*) trapped oil saturation; (*b*) effective relative permeability $k^e_{r_o} = (1 - \zeta/S)S^2$. The model parameters are: $S_{oim} = 0.4$, $S_{wdr} = 0.2$, $\tau_0 = 2.5\tau_g$ and $|\mathrm{d}S/\mathrm{d}t| = 1$.

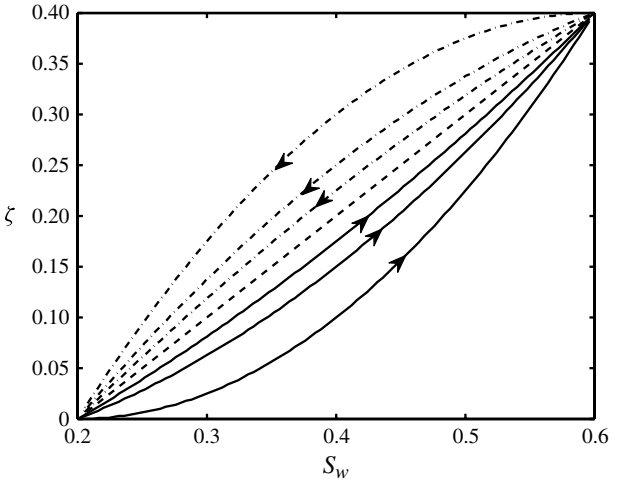

FIGURE 21. Hysteresis loops for trapped oil saturation for three different values of $|\mathrm{d}S/\mathrm{d}t| = 0.25$, 0.5 and 1; primary imbibition, secondary drainage and equilibrium curves are shown by the same line types as in figure 20(*a*). As $|\mathrm{d}S/\mathrm{d}t|$ decreases, the primary imbibition and secondary drainage curves approach the equilibrium curve.

to assume that if oil reaches the residual limit, i.e. if $S = S_{oim}$, the mean trapping rate is infinite and the mean mobilization rate is zero and that if water reaches the irreducible limit, i.e. if $1 - S = S_{wdr}$, the mean trapping rate is zero and the mean mobilization rate is infinite. Consequently, $\zeta^{eq} = S_{oim}$ and $\overline{\tau}_\zeta = 0$ at $S = S_{oim}$, $\zeta^{eq} = 0$ and $\overline{\tau}_\zeta = 0$ at $S = 1 - S_{wdr}$. These end point conditions for ζ^{eq} and $\overline{\tau}_\zeta$ are satisfied by the expressions

$$\zeta^{eq} = S_{oim}\frac{(1 - S_{wdr} - S)}{(1 - S_{wdr} - S_{oim})} \quad \text{and} \quad \overline{\tau}_\zeta = \tau_0(1 - S_{wdr} - S)(S - S_{oim}). \tag{B 6}$$

Hilfer (2006*a*) used a more complex ζ^{eq}–S relationship, which satisfies the same end-point conditions and has monotonically decreasing slope the same as the one above. Figures 20(*a*) and 20(*b*) depict the trapped oil saturation and effective oil

relative permeability, respectively, against water saturation for the successive processes of primary drainage, primary imbibition and secondary drainage, where the arrows indicate the flow directions. The following model parameters were used to obtain these curves: $S_{oim} = 0.4$, $S_{wdr} = 0.2$, $\tau_0 = 2.5\tau_g$ and $|\mathrm{d}S/\mathrm{d}t| = 1$. Moreover, it is assumed that no trapping occurs during primary drainage. During primary imbibition the trapped oil saturation increases from zero to its maximum value, which is achieved at the end of the imbibition process. Consequently, the effective relative permeability is lower during primary imbibition than during primary drainage. During secondary drainage the trapped saturation decreases; however, it follows a path different from the one it followed during the primary imbibition. The trapped saturation is higher during secondary drainage than during primary imbibition; consequently, the relative permeability is lower during secondary drainage than during primary imbibition. The deviation in trapped oil saturation during primary imbibition and secondary drainage from the equilibrium solution (ζ^{eq}) certainly depends on the magnitude of $|\mathrm{d}S/\mathrm{d}t|$ (or $\overline{\tau}_\zeta$); as $|\mathrm{d}S/\mathrm{d}t|$ is decreased, the trapped oil saturation approaches the equilibrium solution (figure 21).

REFERENCES

AHLSTROM, S. W, FOOTE, H. P., ARNETT, R. C., COLE, C. R. & SERNE, R. J. 1977 Multi-component mass transport model: theory and numerical implementation. Rep. Battle Pacific Northwest Laboratories, Richaland, Washington 99352 (USA)-2127..

AMILI, P. & YORTSOS, Y. C. 2006 Darcian dynamics: a new approach to the mobilization of a trapped phase in porous media. *Trans. Porous Med.* **64**, 25–49.

AVRAAM, D. G., KOLONIS, G. B., ROUMELIOTIS, T. C., CONSTANTINIDES, G. N. & PAYATAKES, A. C. 1994 Steady-state two-phase flow through planar and nonplanar model porous media. *Trans. Porous Med.* **16**, 75–101.

AVRAAM, D. G. & PAYATAKES, A. C. 1995*a* Flow rigimes and relative permeabilties during steady-state two-phase flow in porous media. *J. Fluid Mech.* **293**, 207–236.

AVRAAM, D. G. & PAYATAKES, A. C. 1995*b* Generalized relative permeability coefficients during steady-state two-phase flow in porous media, and correlation with the flow mechanisms. *Trans. Porous Med.* **20**, 135–168.

BARENBLATT, G. I., PATZEK, T. W. & SILIN, D. B. 2003 The mathematical model of non-equilibrium effects in water–oil displacement. *Soc. Petrol. Engng J.* **8**, 409–416.

BEAR, J. 1972 *Dynamics of Fluids in Porous Media*. Dover.

BLUNT, M., JACKSON, M. D., PIRI, M. & VALVATNE, P. H. 2002 Detailed physics, predictive capabilities and macroscopic consequences for pore-network models of multiphase flow. *Adv. Water Resour.* **25**, 1069–1089.

CERCIGNANI, C. 1988 *The Boltzmann Equation and its Application*. Springer.

DAHLE, H. K., ESPENDAL, M. S., EWING, R. E & VARIED, O. SÆ 1990 Characteristic adaptive subdomain methods for reservoir flow problems. *Numer. Meth. Partial Differ. Equ.* **6**, 279–309.

DAHLE, H. K., EWING, R. E. & RUSSELL, T. F. 1995 Eulerian–Lagrangian localized adjoint method for a nonlinear advection-diffusion equation. *Comput. Meth. Appl. Mech. Engng* **34**, 1051–1069.

DIAS, M. M. & PAYATAKES, A. C. 1986*a* Network models for two-phase flow in porous media. Part 1. Immiscible microdisplacement of non-wetting fluids. *J. Fluid Mech.* **164**, 305–336.

DIAS, M. M. & PAYATAKES, A. C. 1986*b* Network models for two-phase flow in porous media. Part 2. Motion of oil ganglia. *J. Fluid Mech.* **164**, 337–358.

DULLIEN, F. A. L. 1992 *Porous Media: Fluid Transport and Pore Structure*. Academic.

GARDINER, C. W. 2004 *Handbook of Stochastic Methods*. Springer.

DE GENNES, P. G. 1983 Hydrodynamic dispersion in unsaturated porous media. *J. Fluid Mech.* **136**, 189–200.

DE GENNES, P.-G., BROCHARD-WYART, & QUERE, D. 2004 *Capillarity and Wetting Phenomena: Drops, Bubbles, Pearls, Waves*. Springer.

GILLESPIE, D. T. 1991 *Markov Processes: An Introduction for Physical Scientists*. Academic.

GIOIA, F., ALFANI, G., ANDREUTTI, S. & MURENA, F. 2003 Oil mobility in saturated water-wetted bed of glass-beads. *J. Hazard. Mater.* **B97**, 315–327.

HASSANIZADEH, S. M., CELIA, M. A. & DAHLE, H. K. 2002 Dynamic effect in the capillary pressure-saturation relationship and its impact on unsaturated flow. *Vadose Zone J.* **1**, 38–57.

HEINZ, S. 2004 Molecular to fluid dynamics: the consequences of stochastic molecular motion. *Phys. Rev.* E **70** (3), 036308.

HESSE, M. A. JR., ORR, F. M. & TCHELEPI, H. A. 2008 Gravity currents with residual trapping. *J. Fluid Mech.* **611**, 35–60.

HEWETT, T. A. & YAMADA, T. 1997 Theory for the semianalytic calculation of oil recovery and effective relative permeability using streamtubes. *Adv. Water Resour.* **20**, 279–292.

HILFER, R. 2006*a* Macroscopic capillarity without a constitutive capillary pressure function. *Phyisca* A **371**, 209–225.

HILFER, R. 2006*b* Macroscopic capillary and hysteresis for flow in porous media. *Phys. Rev.* E **73**, 016307.

HINKLEY, R. E., DIAS, M. M. & PAYATAKES, A. C. 1987 On the motion of oil ganglia in porous media. *PhysicoChem. Hydrodyn.* **8** (2), 185–211.

IDE, S. T., JESSEN, K. JR. & ORR, F. M. 2007 Storage of CO_2 in saline aquifers: effects of gravity, viscous and capillary forces on amount and timing of trapping. *Intl J. Greenh. Gas Control* **1**, 481–491.

JENNY, P., POPE, S. B., MURADOGLU, M. & CAUGHEY, D. A. 2001 A hybrid algorithm for the joint p.d.f. equation of turbulent reactive flows. *J. Comput. Phys.* **166**, 218–252.

JENNY, P., TORRILHON, M. & HEINZ, S. 2010 A solution algorithm for the fluid dynamic equations based on a stochastic model for molecular motion. *J. Comput. Phys.* **229**, 1077–1098.

JERAULD, G. R. & SALTER, S. J. 1990 The effect of pore-structure on hysteresis in relative permeability and capillary pressure: pore-level modelling. *Trans. Porous Med.* **5**, 103–151.

JUANES, R., SPITERI, E. J. JR., ORR, F. M. & BLUNT, M. J. 2006 Impact of relatively permeability hysteresis on geological CO_2 storage. *Water Resour. Res.* **42**, W12418.

KATS, F. M. VAN & DUJIN, C. J. VAM 2001 A mathematical model for hysteric two-phase flow in porous media. *Trans. Porous Med.* **43**, 239–263.

KINZELBACH, W. 1992 *Numerische Methoden zur Modellierung des Transports von Schadstoffen im Grundwasser*. Oldenbourg.

KOCH, D. L. & BRADY, J. F. 1987 A non-local description of advection-diffusion with application to dispersion in porous media. *J. Fluid Mech.* **180**, 387–403.

KUMAR, A., OZAH, R., NOH, M., POPE, G. A., BRYANT, S., SEPEHRNOORI, K. & LAKE, L. W. 2005 Reservoir simulation of CO_2 storage in deep saline aquifers. *Soc. Petrol. Engng J.* **10**, 336–348.

LARSON, R. G., SCRIVEN, L. E. & DAVIS, H. T. 1977 Percolation theory of residual phases in porous media. *Nature* **268**, 409–413.

LENHARD, R. J., PARKER, J. C. & KALUARCCHCHI, J. J. 1989 A model for hysteretic constitutive relations governing multi-phase flow 3. Refinements and numerical simulation. *Water Resour. Res.* **25**, 1727–1736.

LENORMAND, R., ZARCONE, C. & SARR, A. 1983 Mechanisms of the displacement of one fluid by another in a network of capillary ducts. *J. Fluid Mech.* **135**, 337–353.

LEVEQUE, R. J. 1992 *Numerical Methods for Conservation Laws. Lectures in Mathematics: ETH Zurich*, Birkhäuser.

MUSKAT, M. 1949 *Physical Princples of Oil Production*. McGraw-Hill.

NAUD, B. 2003 p.d.f. modelling of turbulent sprays and flames using particle stochastic method. PhD thesis, Delft University of Technology, The Netherlands.

NG, K. M., DAVIS, H. T. & SCRIVEN, L. E. 1978 Visualization of blob mechanics in flow through porous media. *Chem. Engng Sci.* **33**, 1009–1017.

NG, K. M. & PAYATAKES, A. C. 1980 Stochastic simulation of the motion, breakup and stranding of oil ganglia on water-wet granular porous media during immiscible displacement. *AIChE J.* **26**, 419–429.

PANFILOV, M. B. & PANFILOVA, I. V. 1995 Macrokinetic model of the trapping process in two-phase fluid displacement in porous media. *Fluid Dyn.* **30**, 409–416.

PAYATAKES, A. C. 1982 Dyanamics of oil ganglia during immiscible displacement in water-wet porous media. *Annu. Rev. Fluid Mech.* **14**, 365–393.

PAYATAKES, A. C., NAG, K. M. & FLUMERFELT, R. W. 1980 Oil ganglion dynamics during immiscible displacement: model formulation. *AIChE J.* **26**, 430–443.

PIRI, M. & BLUNT, M. J. 2005 Three-dimensional mixed-wet random pore-scale network modelling of two- and three-phase flow in porous media. ii. results. *Phys. Rev.* E **71**, 026302–026313.

POPE, S. B. 1985 P.d.f. methods for turbulent reactive flows. *Prog. Energy Combust. Sci.* **11**, 119–192.

POPE, S. B. 2003 *Turbulent Flows*. Cambridge University Press.

PRICKETT, T. A., NAYMIK, T. G & LONGQUIST, C. G 1981 A random walk solute transport model for selected groundwater quality evaluations. Illinois State Water Survey Bulletin 65, Champaign, IL.

REMBOLD, B. & JENNY, P. 2006 A multiblock joint p.d.f. finite-volume hybrid algorithm for the computation of turbulent flows in complex geometries. *J. Comput. Phys.* **220**, 59–87.

RICHARDS, L. A. 1931 Capillary conduction of liquid through porous mediums. *Physics* **1**, 318–333.

ROOF, J. G. 1970 Snap-off of oil droplets in water-wet pores. *Soc. Petrol. Engng J.* **10**, 85–90.

SCHEMBRE, J. M. & KOVSCEK, A. R. 2006 Estimation of dynamic relative permeability and capillary pressure from countercurrent imbibition experiments. *Trans. Porous Med.* **65**, 31–51.

SILIN, D. B. & PATZEK, T. W. 2004 On barenblatt's model of spontaneous countercurrent imbibition. *Trans. Porous Med.* **54**, 297–322.

SPITERI, E. J., JUANES, R., BLUNT, M. J. & ORR, F. M. 2008 A new model of trapping and relative permeability hysteresis for all wettability characteristics. *Soc. Petrol. Engng J.* **13**, 277–288.

TYAGI, M. & JENNY, P. 2011 Probability density function modelling of multi-phase flow in porous media with density-driven gravity currents. *Trans. Porous Med.* **87**, 602–623.

TYAGI, M., JENNY, P., LUNATI, I. & TCHELEPI, H. A. 2008 A stochastic, Lagrangian modelling framework for multi-phase flow in porous media. *J. Comput. Phys.* **227**, 6696–6714.

VALAVANIDES, M. S., CONSTANTINIDES, G. N. & PAYATAKES, A. C. 1998 Mechanistic model of steady-state two-phase flow in porous media based on ganglion dynamics. *Trans. Porous Med.* **30**, 267–299.

WARDLAW, N. C. & MCKELLAR, M. 1985 Oil blob populations and mobilization of trapped oil in unconsolidated packs. *Can. J. Chem. Engng* **63**, 525–532.